Cancer Research

Free Fatty Acids Rewire Cancer Metabolism in Obesity-Associated Breast Cancer via Estrogen Receptor and mTOR Signaling

Zeynep Madak-Erdogan[1,2,3,4,5,6], Shoham Band[1], Yiru C. Zhao[1], Brandi P. Smith[1], Eylem Kulkoyluoglu-Cotul[1], Qianying Zuo[1], Ashlie Santaliz Casiano[2], Kinga Wrobel[1], Gianluigi Rossi[7], Rebecca L. Smith[7], Sung Hoon Kim[8], John A. Katzenellenbogen[8], Mariah L. Johnson[9], Meera Patel[9], Natascia Marino[9,10], Anna Maria V. Storniolo[9,10], and Jodi A. Flaws[11]

Abstract

Obesity is a risk factor for postmenopausal estrogen receptor alpha (ERα)-positive (ER^+) breast cancer. Molecular mechanisms underlying factors from plasma that contribute to this risk and how these mechanisms affect ERα signaling have yet to be elucidated. To identify such mechanisms, we performed whole metabolite and protein profiling in plasma samples from women at high risk for breast cancer, which led us to focus on factors that were differentially present in plasma of obese versus nonobese postmenopausal women. These studies, combined with *in vitro* assays, identified free fatty acids (FFA) as circulating plasma factors that correlated with increased proliferation and aggressiveness in ER^+ breast cancer cells. FFAs activated both the ERα and mTOR pathways and rewired metabolism in breast cancer cells. Pathway preferential estrogen-1 (PaPE-1), which targets ERα and mTOR signaling, was able to block changes induced by FFA and was more effective in the presence of FFA. Collectively, these data suggest a role for obesity-associated gene and metabolic rewiring in providing new targetable vulnerabilities for ER^+ breast cancer in postmenopausal women. Furthermore, they provide a basis for preclinical and clinical trials where the impact of agents that target ERα and mTOR signaling cross-talk would be tested to prevent ER^+ breast cancers in obese postmenopausal women.

Significance: These findings show that obesity-associated changes in certain blood metabolites rewire metabolic programs in cancer cells, influence mammary epithelial cell tumorigenicity and aggressiveness, and increase breast cancer risk.

Introduction

The rate of increase in BMI is higher for women in the United States and percent of cancer cases attributable to excess body weight is twice as high for women compared with men (1, 2). Sedentary lifestyle and western-style, fat- and sugar-rich diets, combined with low estrogen levels in postmenopausal women, aggravate this problem, making postmenopausal women more susceptible to weight gain, fat redistribution to abdominal areas, dyslipidemia, hypertension, and insulin resistance, which are the major hallmarks of metabolic syndrome (3). In fact, almost 70% of postmenopausal women in the United States are overweight or obese. A weight gain of 55 or more pounds from age 18 increases breast cancer risk by 50% (4). Being overweight after menopause increases ER^+ breast cancer risk by 70% (5–7). Eighty-two different studies including analysis of more than 200,000 women with breast cancer showed that obesity increases mortality both in premenopausal and postmenopausal women (8). Obesity-associated cancers are a significant clinical problem and uncovering and targeting obesity-associated molecules and signaling pathways activated by these molecules may identify populations at risk and reduce breast cancer–related deaths.

Systemic hyperlipidemia, hyperglycemia, insulin resistance, increased estrogen production by adipose tissue, and increased inflammation associated with obesity contribute to the risk and development of breast cancer (9). Obesity-associated factors such as IGF1, adipokines, and cytokines modulate oncogenic PI3K and mTOR signaling pathways (10). Tumor-associated cholesterol metabolites, such as 27-hydroxycholesterol, also increased risk of breast cancer metastasis and worsen breast

[1]Department of Food Sciences and Human Nutrition, University of Illinois, Urbana-Champaign, Urbana, Illinois. [2]Division of Nutritional Sciences, University of Illinois, Urbana-Champaign, Urbana, Illinois. [3]National Center for Supercomputing Applications, University of Illinois, Urbana-Champaign, Urbana, Illinois. [4]Cancer Center at Illinois, University of Illinois, Urbana-Champaign, Urbana, Illinois. [5]Beckman Institute for Advanced Science and Technology, University of Illinois at Urbana-Champaign, Urbana, Illinois. [6]Carl R. Woese Institute for Genomic Biology, University of Illinois, Urbana-Champaign, Urbana, Illinois. [7]Department of Pathobiology, University of Illinois, Urbana-Champaign, Urbana, Illinois. [8]Department of Chemistry, University of Illinois, Urbana-Champaign, Urbana, Illinois. [9]Susan G. Komen Tissue Bank at the IU Simon Cancer Center, Indianapolis, Indiana. [10]Department of Medicine, Indiana University School of Medicine, Indianapolis, Indiana. [11]Department of Comparative Biosciences, University of Illinois, Urbana-Champaign, Urbana, Illinois.

Note: Supplementary data for this article are available at Cancer Research Online (http://cancerres.aacrjournals.org/).

Corresponding Author: Zeynep Madak-Erdogan, University of Illinois at Urbana Champaign, 359 ERML Hall, 1201 W. Gregory Dr., Urbana, IL 61801-3704. Phone: 217-300-9063; Fax: 217-265-0925; E-mail: zmadake2@illinois.edu

doi: 10.1158/0008-5472.CAN-18-2849

cancer outcomes (11–13). Yet, we still lack the information regarding other molecules from plasma that increase the breast cancer risk.

Our aim in this study was to identify and test the impact of various circulating factors in blood associated with breast cancer risk. Our hypothesis was that specific circulating metabolites and proteins, detectable in plasma, increase the risk of ER^+ breast cancer in obese postmenopausal women compared with their nonobese counterparts. Using a multiple -omics approach, we identified certain free fatty acids (FFA) that are relevant to obesity-associated breast cancer risk and uncovered ERα and mTOR pathway–dependent metabolic rewiring in breast cancer cells under conditions that mimic plasma from obese postmenopausal women. We have previously described the identification and design of novel pathway preferential estrogens that modulate ERα and mTOR signaling cross-talk (14). One of these compounds, termed pathway preferential estrogen 1 (PaPE-1), was initially identified in a screen of estrogen-like molecules that had lower affinity for the estrogen receptor, and stimulated extranuclear ER activity with limited effects on nuclear ER-target gene expression. PaPE-1 modulated extranuclear ER-initiated kinase signaling, particularly mTOR pathway, without inducing ERα recruitment to chromatin. In *in vivo* experiments, PaPE-1 treatment reduced ovariectomy-induced weight gain, blood triglyceride levels, and fat deposition in an ERα-dependent manner, without stimulating the uterus or mammary gland, and displayed a pattern of metabolic tissue-selective activity that would be optimal for preventing breast cancer in postmenopausal women by reducing fat accumulation in the body (14). In this study, PaPE-1, was able to block FFA-dependent changes in human breast cancer cells. Hence, we have uncovered a novel role for extranuclear-initiated ERα signaling in rewiring breast cancer cell metabolism in response to obesity-associated factors in the plasma. Our findings provide a basis for preventing or inhibiting obesity-associated breast cancer by using PaPEs that would exploit new metabolic vulnerabilities of breast tumors in obese postmenopausal women.

Materials and Methods

Participants and samples

All studies were approved by the Indiana University Institutional Review Board (IRB protocol numbers 1011003097 and 1607623663). All research was carried out in compliance with the Helsinki Declaration. Donors provide broad consent for the use of their specimens in research. The written informed consent document informed the donor that the donated specimens and medical data were going to be used for the general purpose of helping to determine how breast cancer develops. It is explained in the written informed consent that the exact laboratory experiments are unknown at the time of donation, and that proposals for use of the specimens will be reviewed and approved by a panel of independent researchers before specimens and/or data are released for research purposes. Hematoxylin and eosin–stained sections of the formalin-fixed, paraffin-embedded tissue of the identified donors were reviewed by a pathologist to confirm the absence of histologic abnormalities. To exclude or control confounding variables such as age, racial and ethnic background, and menopausal status, the subjects in the two cohorts, susceptible and healthy controls, were matched by selection of the comparison group (healthy controls) with respect to the distribution of the abovementioned confounders in susceptible group.

All studies were approved by the University of Illinois, Urbana-Champaign Institutional Review Board (UIUC IRB protocol number 06741). The Midlife Women's Health Study is a longitudinal study on risk factors for hot flashes in women who are residents of the Baltimore metropolitan region, which includes Baltimore city and several of its surrounding counties (15). This parent study, named the Midlife Women's Health Study, was specifically designed to test the hypothesis that obesity is associated with hot flashes through mechanisms that involve early ovarian failure, altered estradiol levels, and selected genetic polymorphisms in steroidogenic enzymes and steroid hormone receptors. We analyzed plasma samples from 37 nonobese and 63 obese postmenopausal women who were two to three years into menopause at the time of sampling. In addition, we analyzed plasma samples from 21 postmenopausal women who were obese at the initiation of the study and later lost weight.

Plasma preparation

Blood is drawn into the Plasma Separator tube (Vacutainer Venous Blood Collection Tubes: SST* Plasma Separation Tube, Thermo Fisher Scientific, catalog no. 0268396) and gently mixed by inverting the tube five times. Forty-five minutes (±10 minutes) after the blood has been drawn, the Plasma Separator Tube is placed into a minicentrifuge (Eppendorf centrifuge 5702) and centrifuged at 1,200 rcf for 10 minutes at room temperature. A repeater pipet is used to aliquot 600 μL of the plasma into each of five cryogenic vials. Samples are stored at −80°C until use.

Primary cell culture

Primary mammary epithelial cells were isolated from 10 cryopreserved breast biopsies of healthy donors as described previously (16, 17). Briefly, cryopreserved tissue biopsies were thawed in a 100-mm petri dish containing 5 mL of culture medium. The tissue was minced using opposite scalpels and collected in a 15 mL tube containing 13 mL digestion medium (collagenase/hyaluronidase; StemCell Technologies). The digestion mixture was left in agitation on a tube rotator for 2–3 hours at 37°C. After centrifugation at 600 × *g* for 5 minutes and washing step with PBS the digested pellet was suspended in 3 mL of culture medium. The suspension is filtered through a 70-μm cell strainer and plated in a 60-mm petri dish containing a layer of irradiated MEF feeder cells (Applied StemCell), and 2 μL/mL adenine (Sigma Aldrich), and 0.5 μL/mL ROCK inhibitor (Y-27632, Enzo Life Sciences) are added to the culture media (18). Differential trypsinization was used to separate feeder and epithelial cells during passaging.

Immunofluorescence studies in primary mammary epithelial cell cultures

The primary epithelial cells (2.5×10^4) were plated into 8-well culture slides (Corning) and incubated at 37°C for 18 hours. Upon incubation, cells were then fixed in cold methanol:acetone (1:1) and incubated at −20°C for 15 minutes. After washing twice with PBS1X, cells were incubated with blocking buffer (PBS1X, 5% normal goat serum, 0.1% TritonX-100) at room temperature for 1 hour. Cells were then incubated with the following primary antibodies anti-K14 (BioLegend #PRB-155P-100, polyclonal rabbit, 1:1,000) and anti-K18/8 (Cell Signaling Technology, mouse, 1:100) overnight at 4°C. After washing with PBS1×, the cells were incubated with fluorescent anti-mouse (Alexa Fluor 488 anti-

mouse and Alexa Fluor 594 anti-rabbit) secondary antibodies (1:500, Thermo Fisher Scientific) and DAPI (1:1,000) for 2 hours at room temperature. Both the primary and secondary antibodies were diluted in Antibody diluent (Dako, Agilent). Finally, the cells were washed with PBS1× and slides were mounted with a cover glass. Images were acquired using an Olympus Fluoview 1000 confocal microscope. The number of double positive cells and the total number of cells (DAPI) present in a determined area of each of the 14 primary epithelial cell cultures were counted. The percentage of double positive cells were measured as 100% × (Number of $K14^+K18^+$/Number of $DAPI^+$).

Cell culture, ligand treatments, siRNA, and reagents

MCF-7, T47D, BT474, and MDA-MB-231 cells were obtained from ATCC. ERα expression was verified by qPCR, Western blotting, and gene expression. Cell proliferative response to E2 and other estrogens was monitored regularly. Each cell line was monitored for *Mycoplasma* contamination regularly using Mycoplasma Detection Kit (VWR, 89510-164). MCF-7, T47D, and BT474 cells were grown in minimal essential medium (MEM; Sigma), supplemented with 5% calf serum (HyClone), and 100 μg/mL penicillin/streptomycin (Invitrogen). MDA-MB-231 cells were grown in Leibowitz's medium with 10% calf serum (HyClone), and 100 μg/mL penicillin/streptomycin (Invitrogen). PaPE-1 was synthesized as described previously (14). All the FFAs; oleic acid (OA), palmitic acid (PA), stearic acid (SA), and linoleic acid (LA), used in the cell assays were purchased from Sigma-Aldrich. The FFAs were solved in a small amount of DMSO and brought to desired concentration by adding ethanol. Fulvestrant, RAD001 (mTOR inhibitor), 4-OH-tamoxifen, Etomoxir (E1905), 2-DG (D8375), oligomycin (O4876), rotenone (R8875), and UK5099 (PZ0169) were obtained from Sigma-Aldrich. AZD6244 (MEK inhibitor) was obtained from Selleckchem. For siRNA experiments, MCF-7 cells were seeded on 96-well plates at 2×10^3/well concentration in corresponding growth media containing 5% FBS and no antibiotics. Human CD36 (SC-29995),PPARα (SC-36307) and SREBP-1 (sc-36557) siRNAs were obtained from Santa Cruz Biotechnology (Santa Cruz Biotechnology Inc.) and prepared according to the manufacturer's protocol. Cells were transfected with siRNAs in OptiMEM treatment media (Gibco) without antibiotics by using DharmaFECT transfection reagent (Dharmacon Inc.). Control cells were treated with transfection reagent only. All cells were incubated in 37°C, 5% CO_2-containing incubator for 48 hours (mRNA accession codes of CD36 siRNAs are NM_000072, NM_001001547, NM_001001548, NM_001127443, NM_001127444, mRNA accession codes of PPARα siRNAs are NM_001001928, NM_005036 and mRNA accession codes of SREBP-1 siRNAs are NM_001005291, NM_001321096, NM_004176). After 48 hours, cells were treated with 10^{-7} mol/L OA or PA and 10^{-6} mol/L PAPE-1 individually and in combination every 3 days. Cell viability was measured by adding 10% WST-1 reagent/well at the end of 7th day. Each experiment was repeated at least twice with six technical replicates. A one-way ANOVA test was used to test statistical significance of MCF-7 cell viability difference due to OA or PA treatment with or without siRNA for indicated factors. To validate protein knockdown, MCF-7 cells were seeded on 6-well plates at 2×10^5/well in corresponding growth media containing 5% FBS and no antibiotics. Human CD36 (SC-29995), SREBP-1 (sc-36557), and PPARα (SC-36307) siRNAs were obtained from Santa Cruz Biotechnology (Santa Cruz Biotechnology Inc.) and prepared according to the manufacturer's protocol. Cells were transfected with siRNAs in OptiMEM treatment media (Gibco) without antibiotics by using DharmaFECT transfection reagent (Dharmacon Inc.). Control cells were treated with transfection reagent only. All cells were incubated in 37°C, 5% CO_2-containing incubator. After 48 hours, cells were collected and protein expressions were assessed by Western blotting. Each experiment condition was repeated at least twice and the statistical significance of the results were analyzed by a one-way ANOVA test.

Cell proliferation, migration, and mTOR pathway activation assays

For cell proliferation experiments, cells were seeded at 500 cells/well in triplicate (unless otherwise stated) in 96-well plates (19). The cells were treated with vehicle (0.1% ethanol) or indicated doses of ligands and inhibitors at the concentrations indicated on the 2nd and 5th day. On the 7th day, cell proliferation was assessed using WST-1 reagent (Roche) following the manufacturer's instructions. The number of plasma samples assayed (35 obese and 35 nonobese plasma samples) was determined on the basis of the availability of the plasma samples. The day after seeding the cells, treatments were done using the plasma samples that were diluted 1:3 in growth media. For experiments involving estrogens, media without plasma were added to the vehicle (0.1% EtOH) or PaPE-1, fulvestrant, or 4-OH-Tamoxifen to the final concentration of 1.5 μmol/L. One-hundred microliters of the inhibitor–media mix was added to each well. Next, 50 μL of plasma samples were added to bring the final concentration of plasma to 30% and inhibitor concentration to 1 μmol/L. Plasma from same individuals were used in motility and mTOR pathway activation assays. Cell migration was assayed in BT474 cells that were seeded at a density of 5×10^5 cells/mL in 96-well Fluoroblock plates in triplicate. Twenty-four hours after treatment with the media containing 30% plasma from each individual, cell number on the bottom part of the well was monitored by CellTracker dye using the Cytation 5 software Gen5. mTOR pathway activation was assayed in MCF-7 cells. MCF-7 cells were seeded at 10,000 cells/well in 96-well black-sided clear-bottom plates. Cells were treated with the media containing 30% plasma for 45 minutes and then crosslinked using 4% paraformaldehyde for 30 minutes at room temperature. After 1 hour of blocking using Odyssey blocking buffer at room temperature, cells were incubated with 1:200 p-S6 (Ser235/236; #2211, Cell Signaling Technology) antibody overnight at 4°C. After 3× 10-minute PBS–0.1% Tween washes, cells were incubated in 1:500 goat anti-rabbit IRdye 800cw (LI-COR Biosciences) for 1 hour at room temperature. After 3× 10-minute PBS–0.1% Tween and 3× 10-minute PBS washes, cells were incubated with DRAQ5 Fluorescent Probe for signal normalization for 30 minutes at room temperature. After three PBS washes, the signal was detected using LI-COR Odyssey In-Cell Western Module.

Western blotting

Western blot analysis used specific antibodies for β-actin (Sigma Aldrich), p-Akt (Ser473; #4060), total Akt (#9272), p-ERK1/ERK2 (Thr202/Tyr204; #4370), total ERK1/ERK2 (#9102), Phospho-p70 S6 Kinase (Thr421/Ser424; #9204), Phospho-p70 S6 Kinase (Thr389; #9205), p70 S6 kinase (49D7; #2708), p-4EBP1

(T37/46; #2855), and total 4EBP1 (#9644; Cell Signaling Technology). MCF-7 cells were seeded at 5×10^5 cells in 10-cm dishes in growth media. Next day, cells were treated with vehicle, 100 nmol/L OA, PA, LA, or SA for indicated times. Cell lysate was prepared using RIPA buffer. Samples were sonicated three times for 10 seconds to shear the DNA. Ten micrograms of protein was loaded onto 10% SDS gels. Antibodies were used at 1:500 except for β-actin (1:5,000). Proteins were visualized using Odyssey LI-COR Imaging System.

ChIP-seq analysis and verification using qPCR

The ChIP-seq analysis was performed as described previously (14, 20). ERα–DNA or IgG–DNA complexes were immunoprecipitated using ERα-specific HC-20 antibody (Santa Cruz Biotechnology). The ChIP DNA is from three pooled biological replicates. Libraries were prepared according to Illumina Solexa ChIP-Seq sample processing, and single read sequencing was performed using the Illumina HiSeq 2000. Sequences generated were mapped uniquely onto the human genome (hg18) by Bowtie2. The MACS (model-based analysis of ChIP-seq) algorithm was used to identify enriched peak regions (default settings) with a *P* value cutoff of $6.0e^{-7}$ and FDR of 0.01, as we have described. To verify the identified binding sites from ChIP-seq findings, ChIP-qPCR using the isolated DNA was performed using the primers designed to target the binding sites at PgR (chr11:100,904,522-100,905,458), CISH (chr3:50,642,336-50,643,191), and SREBP1c (chr17:17,743,329-17,743,912).

RNA-seq transcriptional profiling

For gene expression analysis, total RNA was extracted from three biological replicates for each ligand treatment using TRIzol reagent and further cleaned using the RNAeasy Kit (QIAGEN). MCF-7 cells were treated with vehicle (0.1% EtOH), 100 nmol/L PA, LA, or SA, or 100 nmol/L OA in presence or absence of 1 μmol/L PaPE-1 for 24 hours. Once the sample quality and replicate reproducibility were verified, samples from each group were subjected to sequencing. RNA at a concentration of 100 ng/μL in nuclease-free water was used for library construction. cDNA libraries were prepared with the mRNA-TruSeq Kit (Illumina, Inc.). Briefly, the poly-A–containing mRNA was purified from total RNA. RNA was fragmented, double-stranded cDNA was generated from fragmented RNA, and adapters were ligated to the ends.

The paired-end read data from the HiSeq 2000 were processed and analyzed through a series of steps. Base calling and demultiplexing of samples within each lane were done with Casava 1.8.2. FASTQ files were trimmed using FASTQ Trimmer (version 1.0.0). TopHat2 (version 0.5) was employed to map paired RNA-Seq reads to version hg19 of the *Homo sapiens* reference genome in the UCSC genome browser in conjunction with the RefSeq genome reference annotation. Gene expression values (raw read counts) from BAM files were calculated using the StrandNGS (version 2.1) Quantification tool. Partial reads were considered and the option of detecting novel genes and exons was selected. Default parameters for finding novel exons and genes were specified. The DESeq normalization algorithm using default values was selected. Differentially expressed genes were then determined by fold change and *P* value with Benjamini and Hochberg multiple test correction for each gene, for each treatment relative to the vehicle control. We considered genes with fold change >2 and *P* value <0.05 as statistically significant, differentially expressed.

OLINK protein biomarker and whole metabolite profiling assays

All the samples from human studies were handled and analyzed in accordance with UIUC IRB protocol #06741. Written informed consent was obtained from all subjects. Ten microliters of plasma samples from Komen Tissue Bank and Midlife Women's Health studies were submitted to OLINK biosciences for cancer and inflammation biomarker analysis. Fifty microliters of plasma samples from both studies and MCF-7 cell pellets that were treated with vehicle, 100 nmol/L OA, 1 μmol/L PaPE-1+OA for 24 hours were submitted to the Metabolomics Center at UIUC. Gas chromatography/mass spectrometry (GC/MS) whole metabolite profiling was performed to detect and quantify the metabolites by using GC/MS analysis. Metabolites were extracted from 50 μL of plasma according to Agilent Inc. application notes. The hentriacontanoic acid was added to each sample as the internal standard prior to derivatization. Metabolite profiles were acquired using an Agilent GC/MS system (Agilent 7890 gas chromatograph, an Agilent 5975 MSD, and an HP 7683B autosampler). The spectra of all chromatogram peaks were evaluated using the AMDIS 2.71 and a custom-built database with 460 unique metabolites. All known artificial peaks were identified and removed prior data mining. To allow comparison between samples, all data were normalized to the internal standard in each chromatogram. Metabolomics data with sample class annotations (healthy and susceptible) were uploaded to the statistical analysis tool of MetaboAnalyst software version 4.0 (21). Features with more than 50% missing values were removed. Data were normalized on the basis of values from "Healthy" samples. Data were log transformed and scaled using Auto scaling feature. VIP scores for top 25 metabolites that discriminate between healthy and susceptible individuals were calculated and displayed using the partial least squares discriminant analysis tool. Heatmap of class averages of 25 metabolites was generated using Heatmap feature using default options for clustering and restricting the data to top 25 metabolites ranked by *t* test. Heatmap for abundance of each metabolite and association with class, menopausal status, and BMI were generated using Cluster3 and visualized using Java TreeView. We calculated the correlation between all identified circulating factors (metabolite and protein) using the Pearson correlation coefficient using R software (R Core Team, 2015). R Code to calculate correlation coefficients and *P* values are available upon request. Correlation coefficients and *P* values were clustered using Cluster3 software and visualized using Treeview Java tool.

Seahorse metabolic profiling experiments

The metabolic profiling was performed using MCF-7 cells following the instructions of Seahorse cell profiler, glycolytic stress, and mitochondrial stress kits. A total of 3×10^4 cells/well were seeded in XF 8-well cell culture mini plates in 80 μL of growth medium. This number was chosen based on achieving close to 100% confluence on the day of Seahorse assay run. Experiments were performed in triplicate at least twice. After 24-hour incubation at 37°C in 5% CO_2, vehicle (0.1 % EtOH) or 100 nmol/L each FFA with and without 1 μmol/L PaPE-1, RAD001, or AZD6244 treatment was added to the cells in 200 μL of growth medium. After 24-hour treatment, the medium from each well was carefully removed and replaced

with 180 μL of assay medium. The assay medium was freshly prepared, and the pH was carefully adjusted right before each assay. The substrate mixing and plate loading was done by strictly following the instructions for each assay: XFp cell energy Phenotype test and Mitostress test. The oxygen consumption rate (OCR) and extracellular acidification rate (ECAR) were measured using Seahorse XFp analyzer. The data were analyzed by Wave software. In parallel, a duplicate of each plate was used for cell counting to monitor cell number changes after 24 hours of treatment with FFAs or inhibitors.

Cignal Finder 45-Pathway and Cignal TF reporter assay

Cignal Finder reporter arrays or individual Cignal TF reporter assays were used to measure the activation of 45 different pathways in MCF-7 cells. Cells were seeded in Cignal Finder 96-well plates at a density of 4×10^4 cells/well in growth medium. Reverse transfection was used to introduce the pathway reporter into cells, following the manufacturer's protocol. Briefly, to each well of the plates, 50 μL OptiMEM was added to resuspend the DNA construct. Then, 50 μL of diluted Addgene transfection reagent, as suggested in the protocol, was added to the mixture. Cells were resuspended in OptiMEM with 10% of fetal bovine serum and 0.1 mmol/L NEAA. Then, 50 μL of the cell suspension was added to each well and mixed well with the DNA construct as well as the transfection reagent. The cells were incubated at 37°C/5% CO_2 for 24 hours. The cells were treated with vehicle, 1 μmol/L PaPE-1, 100 nmol/L OA, and OA+PaPE-1 in growth medium for 24 hours. Immediately after the treatment, luciferase activities were determined by using a Dual-Luciferase reporter assay system from Promega. Briefly, the treatment medium was removed carefully from each well, and the cells were rinsed in PBS. After removing the PBS, 20 μL lysis reagent was added to each well, and the plate was incubated for 15 minutes. Then, 100 μL Luciferase assay reagent II (LAR II) was added to each well, and the luminescent signal was read immediately using Cytation 5 plate reader. After quantifying the firefly luminescence, 100 μL Stop & Glo reagent was added to the same sample following the measurement of luminescent signal. Experiments were repeated twice with duplicates. Transcription activity (Luciferase signal/*Renilla* signal) was calculated and all the data were plotted.

Statistical analyses

Data from *in vitro* cell line studies were analyzed using either a one-way ANOVA model to compare different ligand effects or a two-way-ANOVA model to compare FFA, inhibitor or siRNA effects. For every main effect that was statistically significant at $P < 0.05$, pairwise t tests were conducted to determine which ligand or inhibitor treatment levels were significantly different from each other. For these t tests, the Bonferroni correction was employed to control the experiment-wise type I error rate at $\alpha = 0.05$ followed by Bonferroni *post hoc* test using GraphPad Prism version 6 for Windows, (GraphPad Software, www.graphpad.com). All the values for all the experiments were plotted.

Data availability

RNA-seq data files are deposited under the accession number GSE114372 in GEO database and will become publicly available upon online publishing of the manuscript. Metabolomics, ChIP-Seq, and OLINK analysis datasets will be available from investigators upon request.

Results

Identification of plasma factors from breast cancer–susceptible women

Because obese postmenopausal women have increased ER^+ breast cancer risk, we characterized the molecular changes associated with increased body mass index (BMI) and luminal or basal properties of the normal human mammary tissue from obese versus nonobese women. Primary mammary epithelial cells were isolated from seven healthy (BMI < 25) and eight obese (BMI > 30) subjects. As described previously, basal-like tumor cells, or triple-negative breast cancers, may possess a high degree of plasticity, allowing them to transition between basal, progenitor, and luminal states. These cells express basal keratins, such as K5 and K14, often together with luminal keratins such as K8 and K18 consistent with their plasticity (22). A recent study by Granit and colleagues showed that most tumors contained a majority of cells expressing the luminal marker K18 (>50% in 36 of 45 tumors); as well as cells that coexpressed K18 and K14 (present in 38 of 45 tumors) Moreover, they demonstrate that $K18^+K14^+$ cells possess enhanced tumorigenicity (22). Formation of colonies that contain cells of luminal or basal lineage was followed by keratin 8/18 and keratin 14 staining (Fig. 1A). Epithelial cell cultures from 5 of 8 (71%) obese women showed a reduced number of luminal cells and increased presence of cells in an undifferentiated state (K18 and K14 costaining) as compared with those from donors with BMI less than 30. We found a statistically significant increase in the percentage of K14/K18 costained cells in obese women–derived cell cultures (mean ± SEM = 3.08 ± 1.1) as compared with normal weight–derived cells (mean ± SEM = 0.31 ± 0.3; Fig. 1A). These results suggest an association between high BMI and presence of cancer precursor cells in the breast. To examine the association of BMI and breast cancer risk, we utilized data from a cohort of postmenopausal healthy controls (Healthy) and individuals who were clinically healthy at the time of data collection, but later had a diagnosis of breast cancer (Susceptible; $N = 40$ pairs). To exclude or control confounding variables such as age, and racial and ethnic background, the subjects in the two cohorts were matched by selection of the comparison group (healthy controls) with respect to the distribution of the above-mentioned confounders. BMI of paired individuals from susceptible group was higher compared with that of healthy individuals ($P = 0.04$; Fig. 1B). We also analyzed plasma samples from 29 healthy and 30 breast cancer–susceptible individuals who were clinically healthy at the time of plasma collection, but later had a diagnosis of breast cancer. We performed OLINK biomarker analysis for a panel of inflammation and cancer-related proteins. This analysis showed that several inflammation-associated factors [CD160 (23), CD27 (24), IL12B (25) and TNFRSF19 (26)] and cancer biomarkers [hK8 (27), Nectin4 (28), KLK13 (29) and CTSV (30)] were correlated with BMI only in breast cancer–susceptible individuals, but not in healthy controls (Fig. 1C). In addition, two breast cancer–associated proteins in the plasma, SYND1/SDC1 (31) and TNFRSF6b (32), had significantly elevated normalized protein expression (NPX) scores in susceptible women than healthy women (Fig. 1D). Furthermore, by using whole metabolomics analysis and Metaboanalyst software, we identified top 25 plasma metabolites that discriminated between healthy and susceptible postmenopausal women, and therefore are indicative of breast cancer risk (Fig. 1E). This analysis showed that postmenopausal women who developed breast cancer had

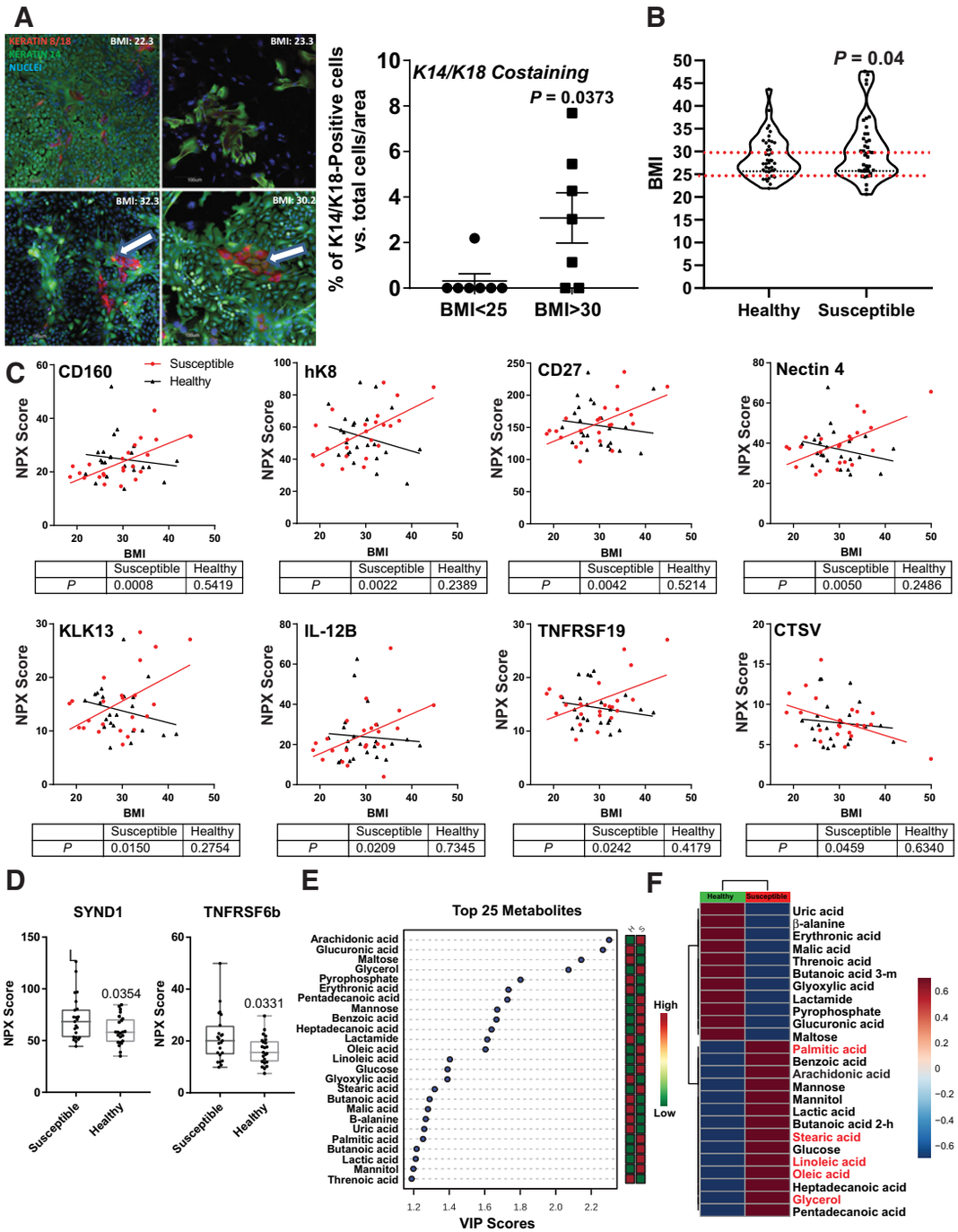

Figure 1.

Identification of plasma factors from breast cancer–susceptible women. **A,** Primary mammary epithelial cultures from women who are BMI < 25 (nonobese) and BMI > 30 (obese). Keratin 8/18 and keratin 14 staining was evaluated by immunofluorescence. Arrows, K14/K18 double-positive cells. **B,** BMI distribution of samples from age, and racial and ethnic background–matched healthy and susceptible individuals ($N = 40$ matched pairs). Paired t test was used to compare BMI for matched healthy and susceptible individuals. **C,** Olink protein biomarker analysis of plasma samples from healthy ($N = 29$) and breast cancer–susceptible ($N = 30$) postmenopausal women. Protein biomarkers that correlate with BMI in susceptible individuals, but not healthy controls, are shown. A linear regression model was generated for BMI and NPX abundance scores of the plasma biomarkers. P values for the significance of nonzero slope of fitted lines are indicated for susceptible and healthy individuals. **D,** Protein biomarkers that are differentially abundant between susceptible versus healthy individuals were identified by t test. P values are indicated. **E,** Top 25 plasma metabolites that distinguish between healthy and susceptible individuals from samples in **B** were identified using biomarker analysis option in web-based MetaboAnalyst software. **F,** Heatmap of the whole metabolite profiling of plasma samples from susceptible and healthy individuals. Heatmap was generated using MetaboAnalyst software.

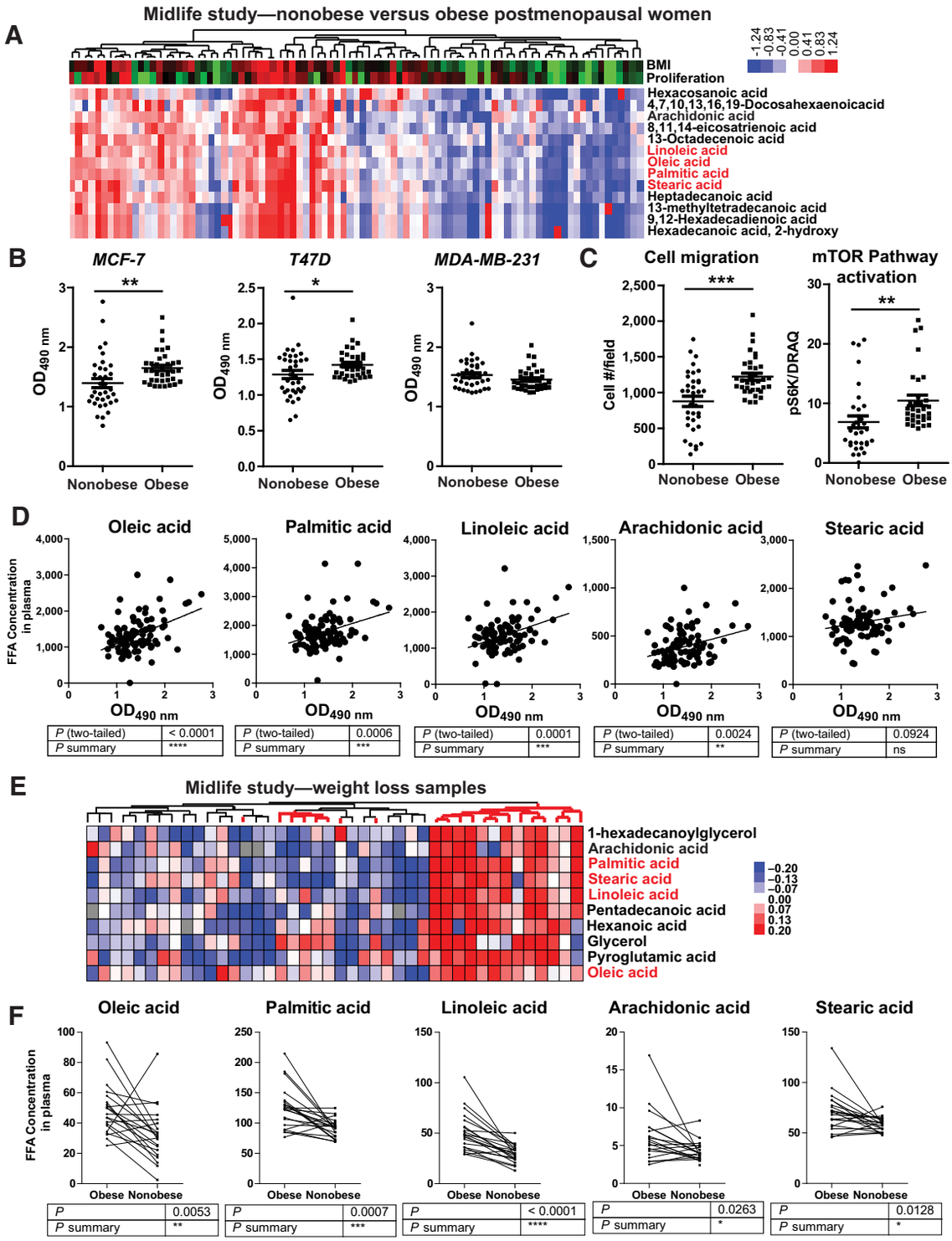

Figure 2.

Validating plasma factors associated with obesity. **A,** Metabolite analysis of plasma samples from 63 obese or overweight versus 37 nonobese postmenopausal women from Midlife Women's Health Study that fits the criteria (2–3 years into menopause), as measured using GC-MS (red, BMI > 25; green, BMI < 25). Cluster 3 software was used to process the data. Raw relative concentration data were log transformed and metabolites (rows), and plasma samples from each individual (columns) were centered to mean. Hierarchical clustering was performed for metabolites and plasma samples using uncentered correlation as similarity metric and complete linkage as clustering method. Data are visualized using Java TreeView software. (*Continued on the following page.*)

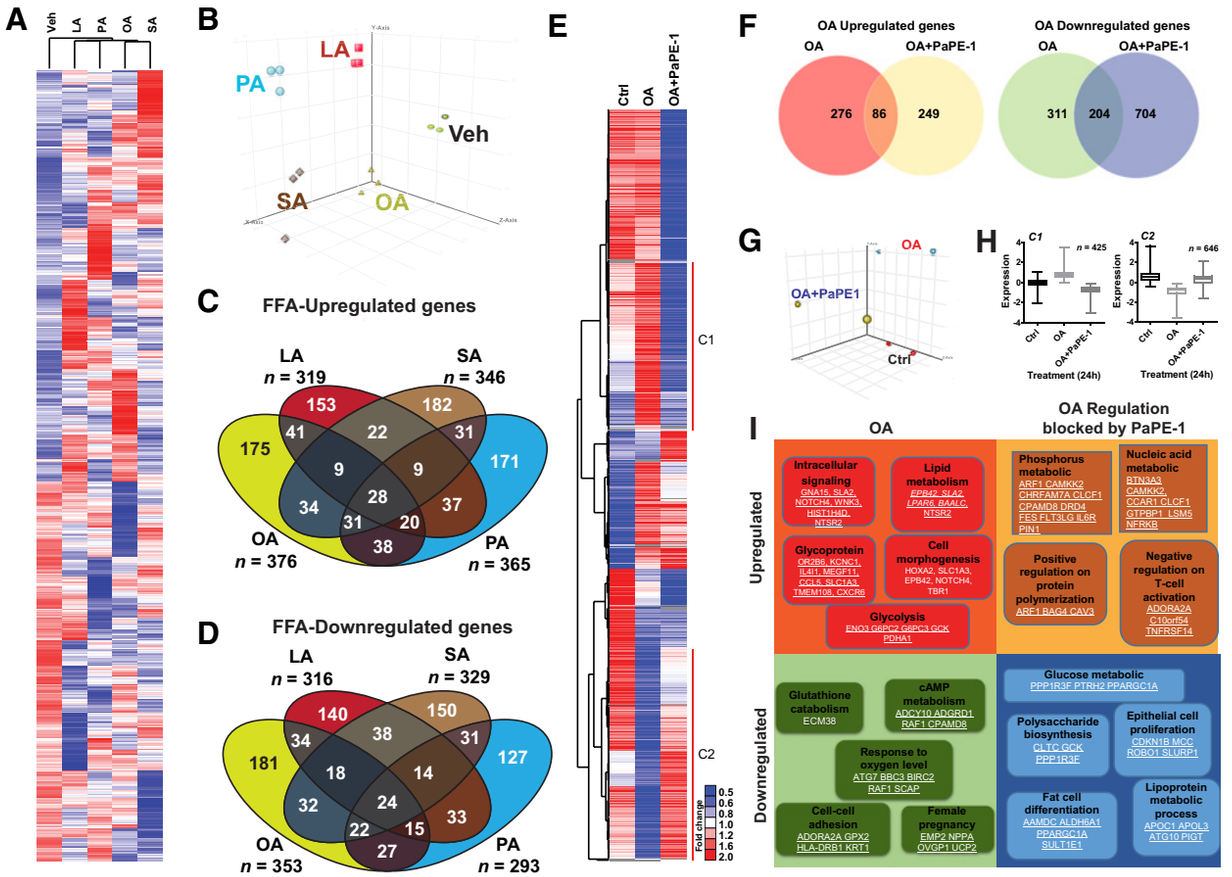

Figure 3.

FFAs induce gene expression changes in breast cancer cells that are blocked by PaPE-1. **A,** Heatmap of RNA-seq analysis of gene expression changes induced by OA, PA, LA, and SA. MCF-7 cells were treated with vehicle or 100 nmol/L of each FFA for 24 hours. RNA was isolated and sequencing was performed using three samples from each treatment group. Differentially expressed genes were determined with $P < 0.05$ and expression fold change >2. **B,** Principal component analysis of gene expression data using differentially expressed genes list from **A**. **C,** Venn diagram analysis showing overlap of genes upregulated by different FFAs. **D,** Venn diagram analysis showing overlap of genes downregulated by different FFAs. **E,** RNA-seq analysis of gene expression changes induced by OA and OA + PaPE-1; heatmap of the genes with significant changed expression. MCF-7 cells were treated with vehicle or 100 nmol/L OA with and without 1 μmol/L PaPE-1 for 24 hours. RNA was isolated and RNA-seq was performed using two samples from each treatment group. Differentially regulated genes were determined with $P < 0.05$ and expression fold change >2. **F,** Venn diagram analysis. Venn diagram of the up- and downregulated genes by OA alone or in combination with PaPE-1. **G,** Principal component analysis of differentially expressed genes from **E**. **H,** Gene expression values of clusters from **E** regulated by OA and reversed by PaPE-1. The average gene expression level of cluster 1 (C1) and 2 (C2) identified as PaPE-1–regulated genes. **I,** Examples of OA-regulated genes. Some of the top functions of the involved genes are presented.

(*Continued.*) Bottom, each column represents a patient and each row represents a metabolite, with elevated levels in red, reduced levels in blue, and mean control levels in white. For BMI and proliferation data, red indicates higher values, whereas green indicates lower values. Bar, the $\log_2$ scale of coloring for normalized metabolite concentrations. **B,** Cell viability assays were performed in both ERα$^+$ and ERα$^-$ breast cancer cell lines. The plasma from 35 obese and 35 nonobese individuals was used to treat the cells for 7 days before analysis by the WST1 assay. Three technical replicates were used. Unpaired *t* test was used to assess whether plasma from obese versus nonobese individuals resulted in statistically significant difference in breast cancer cell line viability. Each point is the average of values from three technical replicates treated with the same plasma samples. *, $P < 0.05$; **, $P < 0.01$. **C,** Cell migration was tested in BT474 cells treated with the plasma samples of 35 obese and 35 nonobese individuals for 24 hours before measurement of cell number per field. The mTOR pathway was found to be activated as indicated by increased pS6K activity by plasma from 35 obese individuals but not by plasma from 35 nonobese individuals in MCF-7 cells. Each point is the average of values from three technical replicates treated with the same plasma samples. Unpaired *t* test was used to assess whether plasma from obese versus nonobese individuals resulted in statistically significant difference in breast cancer cell line motility and mTOR pathway activation. **, $P < 0.01$; ***, $P < 0.001$. Mean ± SEM is plotted. **D,** Pearson correlation analysis of plasma concentrations of FFAs with MCF-7 proliferation from **A**. **E,** Metabolomics analysis of Midlife Women's Health Study-weight loss samples. Initial and final visit plasma samples from 21 postmenopausal women from Midlife Health Study who met the following criteria were analyzed: BMI > 25 at the initial visit and BMI < 25 at the last visit. First visit samples (when individuals were obese or overweight) are indicated with red-thick lines. **F,** Change in the plasma concentrations of FFAs characterized in **E**. An unpaired *t* test was used to assess whether various FFA treatments resulted in statistically significant stimulation of MCF-7 cell proliferation. Individual data points were plotted to indicate the change in FFA concentration after weight loss.

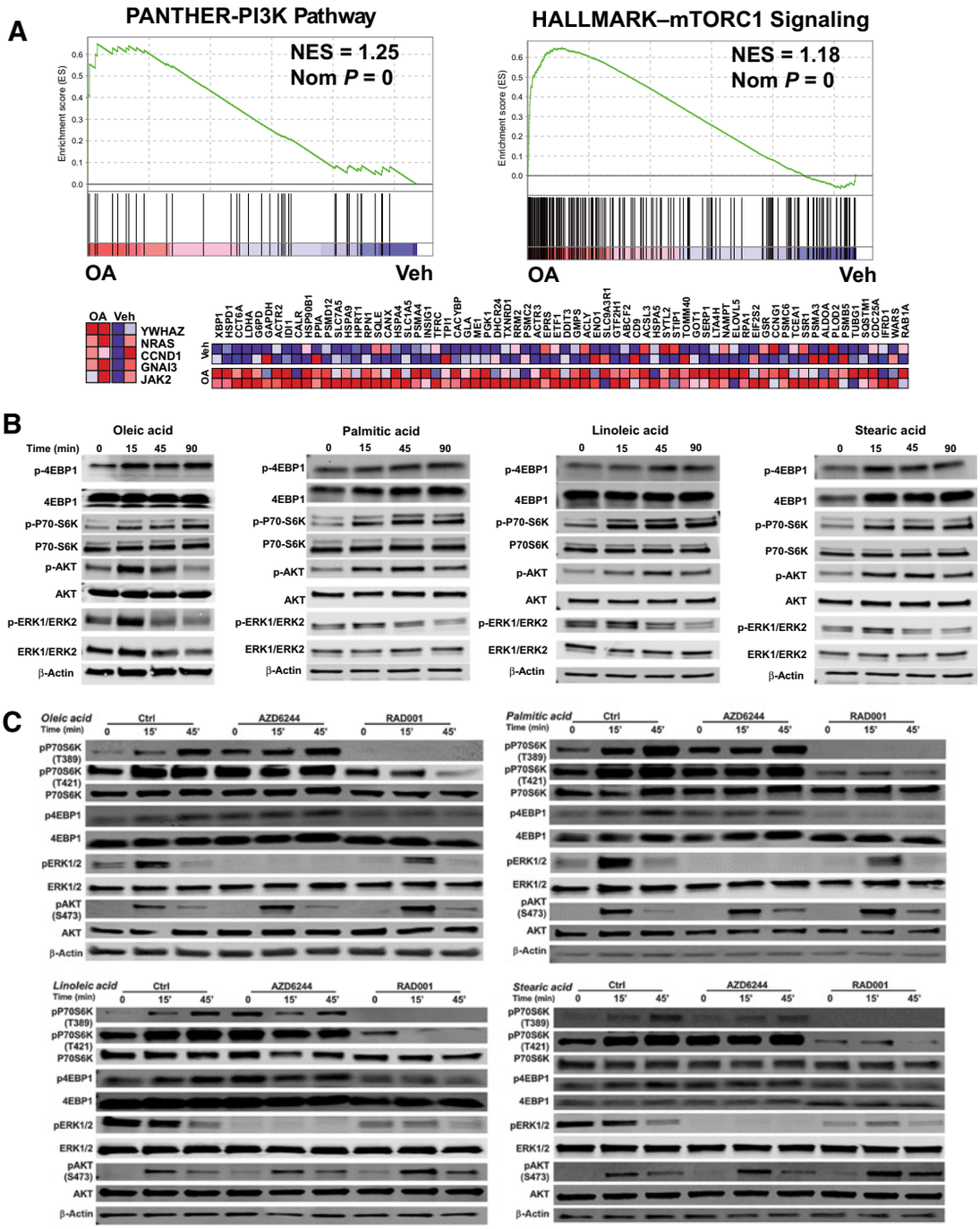

Figure 4.

FFAs activate mTOR and PI3K pathway. **A,** Gene set analysis and identification of mTOR and PI3K pathway–related genes as targets of FFA action. Representative GSEA results and heatmaps for the genes that contribute to the enrichment score. Range of colors (red, pink, light blue, dark blue) correspond to range of expression values (high, moderate, low, lowest). **B,** Time course of protein phosphorylation induced by FFAs. MCF-7 cells were treated with 100 nmol/L OA, PA, LA, or SA for 0, 15, 45, or 90 minutes. Protein lysates were prepared using RIPA buffer. Phosphorylation and total protein levels of AKT, ERK1/ERK2, p70S6K, and 4EBP1 were examined by Western blot analysis. β-Actin was run as internal standard for each blot to ensure equal loading. Antibody signal from phosphorylated proteins was normalized relative to the signal from total protein. The experiment was repeated two times and representative blots are shown. **C,** Impact of pathway inhibitors on FFA-induced signaling pathway changes. MCF-7 cells were pretreated with DMSO vehicle (Ctrl), 1 μmol/L MEK inhibitor AZD6244, or 1 μmol/L mTOR inhibitor RAD001 for 30 minutes. Next, cells were treated with 100 nmol/L OA, PA, LA, or SA for 0, 15, or 45 with or without inhibitors. Protein lysates were prepared using RIPA buffer. Phosphorylation and total protein levels of AKT, ERK1/ERK2, p70S6K, and 4EBP1 were examined by Western blot analysis. The experiment was repeated two times and representative blots are shown.

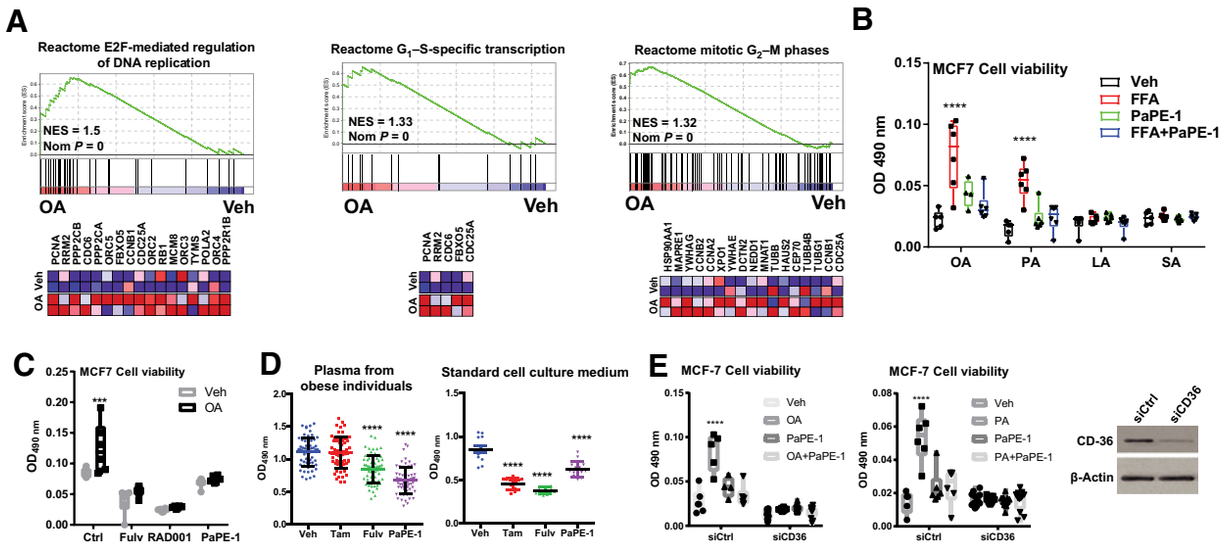

Figure 5.

FFAs induce cell proliferation in an ERα- and CD36-dependent manner. **A,** Representative GSEA results for OA-induced and cell proliferation–associated gene sets and heatmaps for the genes that contribute to the enrichment score. Range of colors (red, pink, light blue, dark blue) corresponds to range of expression values (high, moderate, low, and lowest). **B,** Cell proliferation of MCF-7 cells in the presence of individual FFAs and PaPE-1. Cell proliferation was examined after treatment of cells with FFAs at 100 nmol/L and PaPE-1 at 1 μmol/L. Cells were treated for a week. Six replicates were used in each assay, and the experiment was repeated twice. A two-way ANOVA model was fitted to assess the contribution of ligand (vehicle or FFA) and PaPE-1 treatment on MCF-7 cell proliferation. When the main effects were statistically significant at $\alpha = 0.05$, pairwise *t* tests with a Bonferroni correction were employed to identify whether treatment was statistically different from each other. ****, $P < 0.0001$. All the data from one representative experiment are plotted. **C,** Inhibition of OA-induced MCF-7 cell proliferation by ERα- and mTOR-targeting agents. Cell proliferation was stimulated by 100 nmol/L OA and was suppressed by adding 1 μmol/L fulvestrant (Fulv), mTOR inhibitor 1 μmol/L RAD001, and 1 μmol/L PaPE-1. In the above cell proliferation experiments, MCF-7 cells were treated in whole growth medium by adding the designated compounds. The treatment went for 6 days, and OD at 450 was measured by WST1 assay. The experiment was repeated twice with six technical replicates. A two-way ANOVA model was fitted to assess the contribution of ligand (vehicle or OA) and inhibitor (Ctrl, Fulv, RAD001, and PaPE-1) treatment on MCF-7 cell proliferation. When the main effects were statistically significant at $\alpha = 0.05$, Sidak multiple comparisons test was employed to identify whether treatments were statistically different from each other. ***, $P < 0.0001$. All the data from one representative experiment are plotted. **D,** Inhibition of plasma-induced MCF-7 cell proliferation by 4-OH-tamoxifen (4-OH-tam), fulvestrant, and PaPE-1. The MCF-7 cells were treated with vehicle, 1 μmol/L 4-OH-tamoxifen, 1 μmol/L fulvestrant, and 1 μmol/L PaPE-1 for 6 days before WST-1 assay in 33% plasma from 63 obese individuals (left) and in standard cell culture with 5% FBS (right). There are three technical replicates for each plasma sample and 14 replicates for each treatment in standard cell culture media. A one-way ANOVA model was fitted to assess the contribution of ligands on plasma- or standard cell culture medium–induced MCF-7 cell proliferation. When the main effects were statistically significant at $\alpha = 0.05$, pairwise *t* tests with a Bonferroni correction were employed to identify whether treatments were statistically different from each other. ****, $P < 0.0001$. **E,** Impact of CD36 knockdown on FFA-induced cell proliferation in MCF-7 cells. PPARα was knocked down using siRNA for 48 hours. Impact on OA- and PA-induced cell proliferation was assessed using WST1 assay. Experiment was repeated twice with six technical replicates. A two-way ANOVA model was fitted to assess the contribution of ligand (vehicle, OA, or PA) and siRNA (siCtrl or siCD36) treatment on MCF-7 cell proliferation. When the main effects were statistically significant at $\alpha = 0.05$, pairwise *t* tests with a Bonferroni correction were employed to identify whether treatments were statistically different from each other. ****, $P < 0.0001$. All the data from a representative experiment are plotted.

significantly higher levels of lipolysis byproducts, FFAs, including OA, PA, LA, SA, and arachidonic acid (AA), and glycerol in their plasma as compared with healthy controls (Fig. 1F; Supplementary Fig. S1).

Validating plasma factors associated with obesity

In obese individuals, plasma FFA and glycerol concentrations are higher due to adipose tissue lipolysis (10). Because obesity and increased body fatness are established risk factors for postmenopausal ER$^+$ breast cancer, we focused our analysis on the contribution of FFAs to breast cancer cell properties (33). We measured the circulating FFAs increased in susceptible individuals in an independent cohort including 37 nonobese and 63 overweight and obese (BMI > 25) postmenopausal women from the "Midlife Women's Health Study." Plasma samples were collected from cancer-free women, 2–3 years after onset of menopause (15). Whole metabolite profiling was conducted for these 100 samples (Fig. 2A). The analysis revealed that plasma metabolite composition stratified the samples based on the women's BMI. Because of the lack of medical follow-up for this study, we did not have the data of breast cancer incidence. Therefore, to determine the impact of BMI on cancer cell properties, we evaluated the effect of the plasma samples on cancer cell viability in ERα$^+$ breast cancer cells, MCF7 and T47D, and ERα$^-$, MDA-MB-231 cells (Fig. 2B). Cell viability increase was observed when ERα$^+$, but not ERα$^-$, cells were treated with plasma from obese individuals. There was a statistically significant linear correlation between *in vitro* cell proliferation and plasma donor's BMI, but not with estradiol, testosterone, or progesterone levels (Supplementary Fig. S2A and S2B).

Treatment with plasma from obese women stimulated both BT474 cell line motility and mTOR pathway activation in MCF-7 cells, suggesting a promotion of the aggressive properties of the breast cancer cells (Fig. 2C). Because the original sample set derives from cancer-free women, we measured the levels of several established circulating biomarkers of breast cancer such as lower phenylalanine, glutamate, and isoleucine levels, to verify the

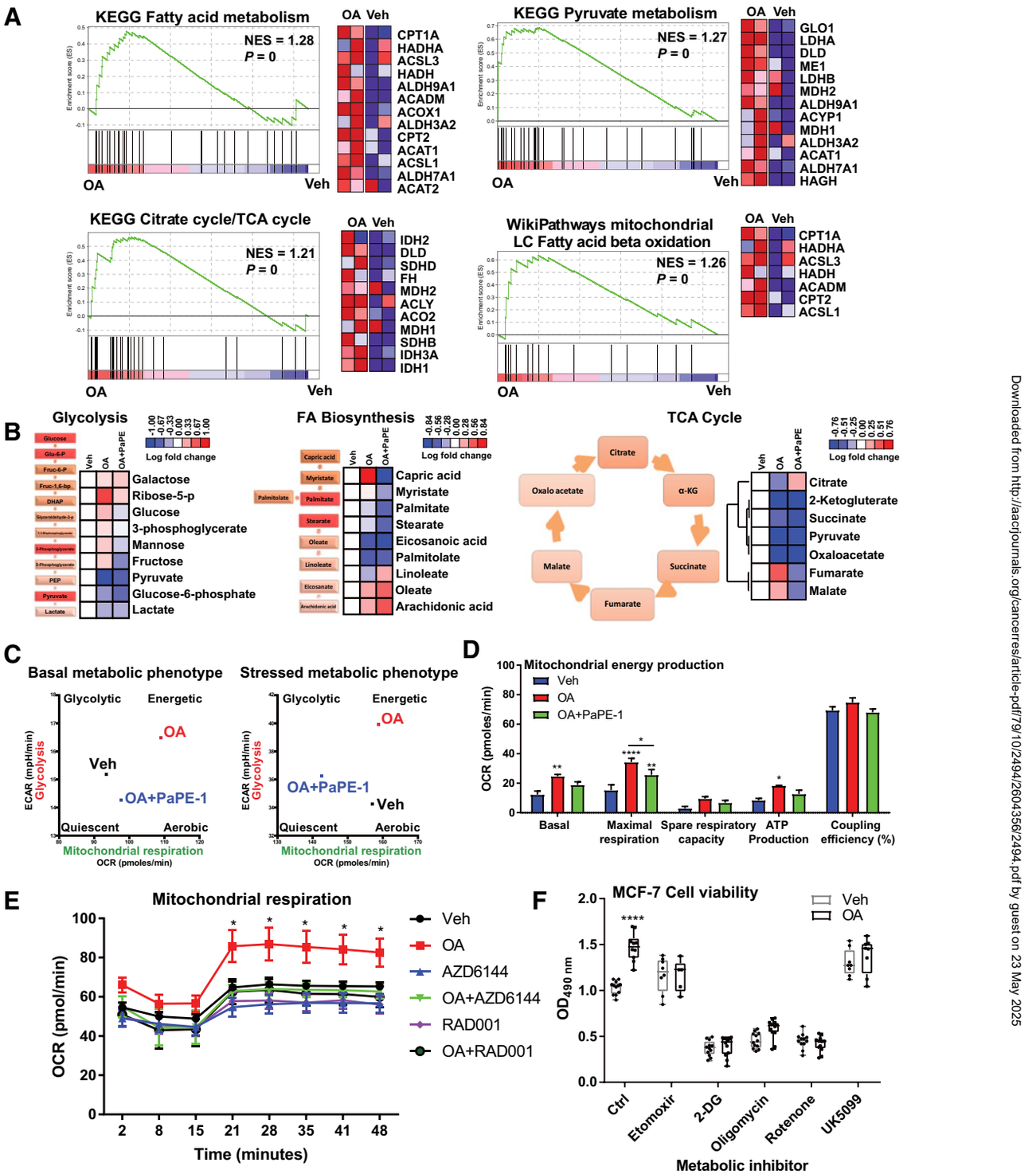

Figure 6.

FFA treatment induces metabolic reprogramming in breast cancer cells. **A,** Examples of GSEA results of metabolic pathways. Representative GSEA results and heatmaps for the genes that contribute to the enrichment score. Range of colors (red, pink, light blue, dark blue) corresponds to range of expression values (high, moderate, low, lowest). **B,** Metabolomics analysis of MCF-7 cells. MCF-7 cells were treated in triplicate using vehicle, 100 nmol/L OA with/without 1 μmol/L PaPE-1 for 24 hours before harvest in cold methanol. Three biological replicates were pooled and submitted for whole metabolite analysis. Data are shown for specific metabolic pathways identified by GSEA analysis and Metscape plugin of Cytoscape. (*Continued on the following page.*)

ability of any newly identified molecules of predicting the breast cancer outcome (34–36). Plasma samples increasing MCF-7 cell viability also showed lower level of the known metabolic cancer biomarkers compared with plasma samples associated with a lower MCF-7 proliferation (Supplementary Fig. S2C). Hence, together, the evaluation of cell viability, motility, and mTOR pathway activation was informative of the breast cancer outcomes. Plasma from overweight or obese women contained higher levels of FFAs similar to those increased in susceptible subjects (Fig. 2A). In addition, MCF-7 cell viability increased with increasing plasma concentration of OA ($P < 0.0001$), PA ($P = 0.0006$), LA ($P = 0.0001$), and AA ($P = 0.002$). Even though there was a trend for SA ($P = 0.09$) the correlation did not reach significance (Fig. 2D). In the "Midlife Women's Health Study", 21 individuals who were obese at the beginning of the study had later lost a significant amount of weight. We monitored circulating FFA levels in these subjects and found significant reduction in all five FFAs upon weight loss when compared with their initial samples (Fig. 2E and F).

FFAs induce gene expression changes in breast cancer cells that are blocked by PaPE-1

To study the impact of FFAs on breast cancer cells, we performed RNA-seq analysis in MCF-7 breast cancer cells treated with vehicle or 100 nmol/L of each FFAs; OA, LA, PA, and SA (Fig. 3A). Each of the FFAs regulated common as well as different groups of genes (Fig. 3B–D). Because plasma from obese patients increased cell viability (Fig. 2B) and mTOR pathway activation (Fig. 2C) in ER^+ breast cancer cells, we further investigated the mechanism of FFAs action using a novel class of compounds, PaPEs. In our previous studies, we showed that PaPEs modulated ERα–mTOR pathway cross-talk and prevented lipid deposition in the liver in mice (14). OA is one of the FFAs with highest blood concentration in patients with breast cancer and was found to be released in highest amounts from the neighboring adipose tissue of mammary epithelial cells upon lipolysis (37–39). Thus, to identify gene expression changes associated with FFA-induced ERα and mTOR pathway modulation, we treated MCF-7 cells with vehicle (Ctrl), 100 nmol/L OA, and 100 nmol/L OA in the presence of 1 μmol/L PaPE-1 (Fig. 3E). The two treatments regulated a substantial number of different genes while also similarly affected overlapping genes (Fig. 3F). PCA analysis shows the appreciable differentiation in gene regulation among the three treatments (Fig. 3G). In cluster 1 (C1), OA upregulated about 350 genes, and activation of 76% of these upregulated genes was blocked by PaPE-1. On the other hand, in cluster 2 (C2), about 500 genes were downregulated by OA, and PaPE-1 was able to restore expression of about 60% of these genes (Fig. 3E and H). GO term analysis showed that OA upregulated those genes that were involved in glycolysis, energy-reserve metabolic process, and epithelial cell migration. On the other hand, OA treatment downregulated those genes that were involved in glutathione and fatty acid metabolism, cell–cell adhesion, and inhibitors of epithelial cell proliferation (Fig. 3I).

FFAs activate mTOR and PI3K pathway

Because plasma from obese individuals also increases mTOR pathway activation (Fig. 2C) and OA upregulated gene sets associated with mTORC1 signaling and PI3K pathway (Fig. 4A), a pathway activation assay was performed to measure activation of mTOR pathway downstream targets P70S6K, and 4EBP1, Akt, and ERK1/ERK2 when cells were treated with individual FFAs (Fig. 4B). The Western blots showed robust and consistent activation of mTOR pathway from OA, PA, LA, and SA treatments as evidenced by increased p70S6K phosphorylation as early as 15 minutes of FFA treatment (Fig. 4B). Longer stimulation with FFAs showed a more robust activation of mTOR pathway. ERK1/ERK2 activation was early and transient as its signal at 45- and 90-minute stimulation return to the baseline (Time 0) level. Fold change of phosphorylation relative to vehicle-treated samples varied by each FFA treatment (Fig. 4B; Supplementary Fig. S3). FFA-dependent activation of both mTOR and MAPK pathway downstream targets were inhibited by mTOR inhibitor RAD001. However, MEK inhibitor AZD6244 only blocked phosphorylation of ERK1 and ERK2 (Fig. 4C).

FFAs induce cell proliferation in an ERα- and CD36-dependent manner

OA treatment decreased expression of inhibitors of epithelial cell proliferation (Fig. 3I) and increased expression of gene sets involved in cell proliferation when compared with control samples (Fig. 5A). Expression of cell-cycle genes regulating transition of the cell through mitotic phases is upregulated by OA (Fig. 5A). OA and PA treatments significantly increased cell viability.

(*Continued.*) For glycolysis, fatty acid biosynthesis and TCA cycle levels of affected substrates and their position in the pathway are shown. Red indicates upregulation and blue indicates downregulation of the abundance of indicated metabolite in the associated pathways. **C,** Cell metabolic phenotype assay using the Seahorse Cell Energy Phenotype Kit. Cells treated with vehicle, OA, and OA + PaPE-1 for 24 hours were tested for the energy phenotype at basal level (left) and under metabolic stress upon inhibition of glycolysis or mitochondrial activity (right). Each experiment was replicated twice with three technical replicates. Results from a representative experiment are shown. **D,** OA treatment increases basal and maximal respiration as well as ATP production. Mitochondrial energy production was measured using the Mitostress kit. Cells were treated in the same way as in Fig. 6C. Various mitochondrial respiration parameters were calculated, as described in Mitostress assay. A two-way ANOVA model was fitted to assess the contribution of ligands on basal and maximal respiration, spare respiration capacity, ATP production, and coupling efficiency. When the main effects were statistically significant at $\alpha = 0.05$, a Tukey multiple comparisons test was employed to identify whether treatments were statistically different from each other. *, $P < 0.05$; **, $P < 0.0001$; ****, $P < 0.0001$. Each experiment was replicated twice with three technical replicates. Results from a representative experiment are shown. **E,** OA-dependent mitochondrial respiration changes are mediated through mTOR and MAPK signaling pathways. MCF-7 cells were treated with 100 nmol/L OA in the presence or absence of 1 μmol/L AZD6244 or RAD001 for 24 hours. Mitochondrial respiration was measured using Seahorse Cell Energy Phenotype Kit. A two-way ANOVA model was fitted to assess the contribution of FFAs to oxygen coupling rate (OCR) over time. When the main effects were statistically significant at $\alpha = 0.05$, a Dunnett multiple comparisons test was employed to identify whether treatments were statistically different from vehicle. *, $P < 0.05$. Each experiment was repeated twice with three technical replicates. **F,** MCF-7 cell viability assay in the presence of OA and various metabolic pathway inhibitors. MCF-7 cells were treated with vehicle or 100 nmol/L OA in the presence or absence of 4 μmol/L etomoxir, 1 mmol/L 2-DG, 50 nmol/L oligomycin, 20 nmol/L rotenone, or 2 μmol/L UK5099 for 6 days. Treatments were repeated on day 3, and cell viability was measured using MTS assay on day 6. A two-way ANOVA model was fitted to assess the contribution of inhibitors on OA-induced cell viability. When the main effects were statistically significant at $\alpha = 0.05$, a Tukey multiple comparisons test was employed to identify whether treatments were statistically different from each other. ****, $P < 0.0001$. All the data are plotted.

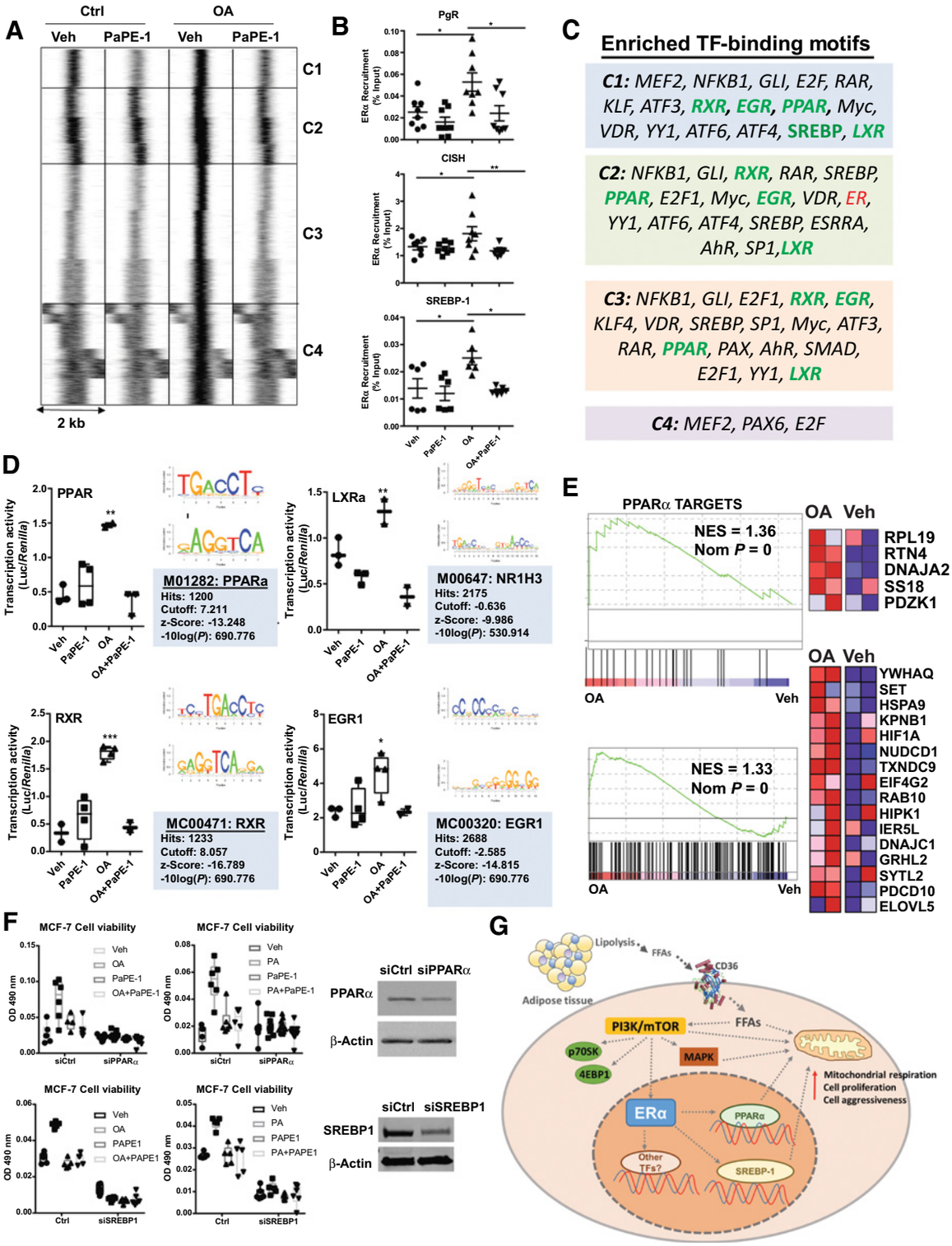

Figure 7.

FFA treatment induces recruitment of ERα to chromatin. **A,** Recruitment of ERα to chromatin in the presence of PaPE-1, OA, and OA + PaPE-1. MCF-7 cells were treated with vehicle and 100 nmol/L OA with or without 1 μmol/L PaPE-1 for 45 minutes. ERα–DNA complexes were pulled down using ERα antibodies. Three biological replicates were pooled and sequenced. Clustering of ERα-binding sites in treatments of vehicle (0.1% EtOH), PaPE-1 (1 μmol/L), OA (100 nmol/L), and OA (100 nmol/L) + PaPE-1 (1 μmol/L) was done using seqMINER software. (*Continued on the following page.*)

However, when cotreated with PaPE-1, the effect of FFAs are markedly reduced (Fig. 5B). To confirm that OA-increased cell proliferation occurred through ERα and mTOR pathways, a cell viability assay was performed with OA treatments in the presence of fulvestrant, an ERα antagonist, and RAD001, an mTOR pathway inhibitor and PaPE-1. All of the tested agents blocked OA-induced cell proliferation, revealing the dependence of the OA-induced cell proliferation on the ERα and mTOR pathways (Fig. 5C). To evaluate whether also plasma from obese individuals induced MCF-7 cell proliferation through ERα and mTOR pathways, cell proliferation assays with plasma samples were performed in the presence of 4-OH-tamoxifen, fulvestrant, and PaPE-1. Notably, PaPE-1 was the most effective agent in inhibiting plasma-induced proliferation of MCF-7 cells (Fig. 5D, left). However, in standard cell culture conditions with 5% FBS, 4-OH-Tamoxifen and fulvestrant showed a stronger inhibition on cell proliferation than PaPE-1 (Fig. 5D, right). These results suggest that treatment with the plasma from obese individuals makes MCF-7 cells more vulnerable to the growth-inhibitory effect of PaPE-1. Increase in MCF-7 cell viability upon OA and PA treatments was blocked in the cells knocked down for CD36, a membrane protein that imports FFAs to the cell (Fig. 5E). These data indicate that FFAs need to be transported inside the cell to stimulate cell proliferation.

FFA treatment induces metabolic reprogramming in breast cancer cells

Gene expression analysis (Fig. 3) pointed out a potential change in metabolic pathways in MCF-7 cells upon OA exposure (Fig. 6A). Metabolomics analysis of MCF-7 cells showed that after OA treatment, glycolysis metabolites were overall increased. Metabolites in the fatty acid biosynthetic pathways were downregulated, suggesting a negative feedback loop due to high levels of extracellular OA (Fig. 6B). OA also downregulated many of the TCA cycle metabolites except malate and fumarate, suggesting an increase in malate shunt from the cytosol (Fig. 6B). Cell metabolic phenotyping assays were performed, which revealed that in the presence of OA, the cells adopted an energetic phenotype and coped with the metabolic stress better by increasing their aerobic and glycolytic metabolic potential. The cells were more glycolytic and their mitochondrial metabolism was increased, but PaPE-1 treatment was able to reverse OA-induced glycolytic and aerobic respiration (Fig. 6C). There was a statistically significant OA-dependent increase in basal and maximal respiration and ATP production, which were reduced by PaPE-1 (Fig. 6D). Inhibition of MAPK and mTOR pathways using small-molecule inhibitors reduced OA-induced changes in mitochondrial respiration (Fig. 6E). To understand the role of metabolism pathways in OA-induced cell proliferation, cells were treated with OA in addition to Etomoxir (a fatty acid oxidation inhibitor), 2-deoxy-D-glucose (2-DG, a glycolysis inhibitor), oligomycin (an ATP synthase inhibitor), Rotenone (an inhibitor of mitochondrial respiration), and UK5099 (an inhibitor of mitochondrial pyruvate transporter). All inhibitors blocked the effects of OA, indicating glycolysis and mitochondrial respiration as key pathways targeted by OA (Fig. 6F).

FFA treatment induces recruitment of ERα to chromatin

To test whether any of the gene expression changes induced by OA treatment occurs through direct ERα recruitment to chromatin, a ChIP-seq experiment was performed. ERα is recruited to novel chromatin sites upon OA treatment and most of this recruitment is blocked by PaPE-1 treatment (Fig. 7A). This ERα recruitment pattern to various sites was verified, including to the classic ERα-binding sites of PgR, CISH, and SREBP-1, the last being a regulator of FA production (Fig. 7B). To understand the nature of ERα recruitment to chromatin in the presence of OA, we further analyzed the OA-induced ERα-binding sites (Fig. 7A and C). This resulted in four main clusters that were named C1, C2, C3, and C4 (Fig. 7C). Transcription factor binding motif enrichment analysis was performed using Seqpos tool from Cistrome/Galaxy. Interestingly, none of the clusters, except C2, had any enrichment of EREs, suggesting a potential tethering mode of recruitment for ERα to these sites (Fig. 7C). Transcriptional activity of some of the previous factors was analyzed with luciferase-based system called Cignal Finder assay (Fig. 7D). Consistent with transcription factor–binding site analysis (Fig. 7C), exposure to OA significantly increased the transcriptional activities of PPAR, LXR, RXR, and

(*Continued.*) Binding sites whose ERα occupation increased upon OA treatment are shown. The ERα-binding sites were separated into four clusters of characteristic patterns: C1, C2, C3, and C4. **B,** Validation of effect of OA and PaPE-1 on the ERα binding at regulatory region of PgR, CISH, and SREBP1C using ChIP-qPCR. MCF-7 cells were treated with vehicle and 100 nmol/L OA with or without 1 μmol/L PaPE-1 for 45 minutes. ERα–DNA complexes were pulled down using ERα antibodies. Recruitment of ERα to PgR (chr11:100,904,522-100,905,458), CISH (chr3:50,642,336-50,643,191), and SREBP1 (chr17:17,743,329-17,743,912) sites was quantified by qPCR. The experiment was repeated three times with at least duplicates each time. Mean ± SEM is plotted. A one-way ANOVA model was fitted to assess the contribution of ligand (vehicle or OA) and inhibitor (Ctrl, PaPE-1) treatment on MCF-7 cell proliferation. When the main effects were statistically significant at $\alpha = 0.05$, pairwise *t* tests with a Bonferroni correction were employed to identify whether treatments were statistically different from each other. *, $P < 0.05$; **, $P < 0.01$. All the data are plotted. **C,** Transcription factor (TF)-binding site enrichment was identified using Seqpos tool from Cistrome/Galaxy for clusters of C1, C2, C3, and C4. **D,** Changes in the transcriptional activities of various transcription factors in the presence of OA and OA+PaPE-1. 45 pathway Cignal Finder Assay was used to transfect MCF-7 cells with indicated luciferase construct for 24 hours. Cells were treated with vehicle and 100 nmol/L OA with or without 1 μmol/L PaPE-1 for 24 hours before measurement by luciferase assay. The experiment was replicated two times with technical duplicates. The transcription factor activity, transcription factor motif, and statistics are shown in detail for PPAR, LXRα, RXR, and EGR1. An unpaired *t* test was used to assess the impact of treatment (OA) and inhibitor (PaPE-1) on transcription factor activity in MCF-7 cells. *, $P < 0.05$; **, $P < 0.01$; ***, $P < 0.001$. All the data are plotted. **E,** GSEA example of PPARα and SREBP1 target genes that are regulated by OA. Representative GSEA results and heatmaps for the genes that contribute to the enrichment score. Range of colors (red, pink, light blue, dark blue) corresponds to range of expression values (high, moderate, low, lowest). **F,** Impact of PPARα (top) or SREBP-1 (bottom) knockdown on FFA-induced cell proliferation in MCF-7 cells. PPARα and SREBP1 were knocked down using siRNA for 48 hours. Impact on OA- and PA-induced cell proliferation was assessed using WST1 assay. Experiment was repeated twice with six technical replicates. A two-way ANOVA model was fitted to assess the contribution of ligand (vehicle, OA, or PA) and siRNA (siCtrl or siPPARα) treatment on MCF-7 cell proliferation. When the main effects were statistically significant at $\alpha = 0.05$, pairwise *t* tests with a Bonferroni correction were employed to identify whether treatments were statistically different from each other. All the data are plotted. **G,** Proposed mechanism for obesity-associated postmenopausal ER^+ breast cancer. Because of increased lipolysis from adipocytes, circulating FFA levels increase in plasma. FFAs are taken up by breast cancer cells in a CD36-dependent manner, which results in activation of mTOR and MAPK signaling and ERα recruitment to chromatin to increase transcriptional activity of factors that regulate cancer cell metabolism. Overall, these upstream events increase mitochondrial respiration, cell proliferation, and aggressiveness for breast cancer cells.

EGR (Fig. 7D). PPARα and SREBP1 target genes, regulating FFA metabolism, are upregulated when treated with OA and result in a significant increase in cell proliferation (Fig. 7E). Knockdown of PPARα and SREBP1 in MCF-7 cells blocked cell proliferation upon OA and PA treatments (Fig. 7F). These analyses suggest that ERα recruits and collaborates with these nuclear receptors to regulate gene expression, resulting in changes that are essential for metabolic processes and survival of breast cancer cells.

Discussion

Our study provides direct evidence for the impact of circulating obesity-associated factors, with a focus on FFAs from plasma, on ERα–mTOR signaling cross-talk in breast cancer. Our combined -omics approach has highlighted gene, metabolite, and transcription factor activity changes that are modulated by circulating factors from blood and for the first time describes obesity-associated metabolic rewiring of breast cancer metabolism related to disease risk that provides new targetable vulnerabilities that we have investigated. We showed that circulating FFA levels are higher in postmenopausal women with high BMI and high breast cancer risk. Circulating FFAs are taken up into cells in a CD36-dependent manner, which results in activation of mTOR and MAPK signaling and ERα recruitment to chromatin to increase transcriptional activity of factors that regulate cancer cell metabolism. Overall, these upstream events increase mitochondrial respiration, cell proliferation, and aggressiveness for breast cancer cells (Fig. 7G).

Obesity causes systemic changes in the body and modifies plasma composition that enables breast cancer cells to thrive in an energy source–abundant, proinflammatory environment. Several studies show that obese patients are more likely to present with advanced-stage disease, derive less benefit from adjuvant systemic therapy, are more likely to develop distant metastases, and die from breast cancer more often than normal weight or underweight patients (40–42). Kerlikowske found that heavily obese (body mass index $\geq$35.0 kg/m^2) postmenopausal women not taking hormone replacement therapy had increased OR for DCIS (OR = 1.46) relative to normal weight women after adjustment for race, ethnicity, age, mammography use, and registry (43). A recent report by Hao and colleagues showed that circulating A-FABP released by adipose tissue directly targeted mammary tumor cells, enhancing tumor stemness and aggressiveness (44).

Previous studies of cancer biomarkers used single metabolomics or proteomics approaches (34, 35), and studies of obesity and breast cancer have focused mainly on changes occurring within the tumor tissue itself (9). Obesity is a pathologic condition characterized by systemic inflammation and physiologic changes that affect the body globally. Thus, we took a broader view by investigating a large number of the plasma-associated factors that revealed associations with obesity: our analysis of plasma of women at high-risk of breast cancer (susceptible) identified metabolites and proteins that potentially drive breast cancer proliferation and aggressiveness and we validated the presence of the same FFAs in the plasma of obese postmenopausal women. Two proteins commonly found to be highly abundant in patients with breast cancer, SYND1/SDC1 (31) and TNFRSF6b (32), were also found to be elevated in the plasma of susceptible subjects. In addition, we showed that the levels of CD160 (23), CD27 (24), IL12B (25), TNFRSF19 (26), hK8 (27), Nectin4 (28), KLK13 (29) and CTSV (30) correlated with BMI in susceptible individuals, but not in healthy controls. Hence, our findings supported a number of BMI-associated biochemical changes in plasma from individuals with high breast cancer risk.

We found that FFAs are major factors affecting breast cancer phenotypic properties through ERα and mTOR signaling. Our observations are consistent with other previously published metabolomics studies that show that same FFA levels are very high in the plasma of patients with breast cancer and that OA and PA are the free fatty acids released in highest amounts from the neighboring adipose tissue of mammary epithelial cells (37–39, 45). It is also possible that increased local estrogen synthesis from adipocytes in the mammary gland might contribute to breast cancer risk, yet we have not identified any association with circulating hormone levels. Consistent with previous studies, we found that OA- and PA-induced changes in cell viability were CD36 dependent (46, 47). CD36 is the transporter required for unbound FFA uptake into the cell. Unbound FFAs are physiologically active, whereas albumin-bound FFAs cannot enter the cells, and interact with the target molecules. FFA concentrations that elicit observed responses are around 100 nmol/L, which is typical for what is determined for unbound FFAs in the plasma (as opposed to millimolar concentration of albumin bound FFAs; ref. 48). In addition, a recent study, targeting the fatty acid receptor CD36 showed that metastasis-initiating cells rely on free fatty acids to promote metastasis (49). Of note, the OA levels we measured were the third highest in the plasma after PA and SA, and SA was not as effective in inducing breast cancer cell proliferation.

OA induced a significant metabolic reprogramming in breast cancer cells. Activation of mTOR signaling provided us with a new metabolic vulnerability point to target obesity-induced breast cancer using novel ERα ligands that modulate mTOR signaling. Previous studies also showed higher mTOR signaling in obesity-associated cancers and pathophysiologic conditions (9, 50–53). We previously showed that ERα and mTORC1 formed a complex upon activation extranuclear–ER signaling (14). Studies from other laboratories suggest that FFAs activate mTOR signaling by *de novo* synthesis of phosphatidic acid (54, 55). Inhibition of mTOR activity by RAD001 blocked p70S6K and 4EBP1 phosphorylation as well as activation of ERK1 and ERK2 by FFAs. On the other hand, inhibition of MEK activity by AZD6244 did not impact mTOR pathway activation, further supporting action of FFAs primarily by changing mTOR pathway activity. Using metabolite and metabolic phenotype profiling, we showed that OA induced a highly energetic phenotype in breast cancer cells, increased glycolytic and aerobic respiration, and modulated key metabolic pathways in these cancer cells through activation of mTOR and MAPK signaling. Because PaPE-1 targets ERα–mTOR signaling (14), this compound resulted in very effective blocking of the OA-induced changes. Our findings have established the scientific basis for future preclinical and clinical studies to firmly establish the impact of FFAs on ER$^+$ breast cancer risk and the clinical utility of agents such as PaPE1 that target ERα and mTOR signaling in prevention of obesity-associated breast cancer. Of note, our data suggested reducing BMI to less than 25 was successful in reducing circulating levels of these factors and further emphasized importance of weight loss strategies to improve quality of life and reduce comorbidities, including ER$^+$ breast cancer in obese postmenopausal women.

In conclusion, our clinical data, combined with cell line models and integrated -omics approaches, provided direct evidence for

the mechanistic involvement of FFAs, particularly OA, in increasing ERα$^+$ breast cancer proliferation and aggressiveness in obese postmenopausal women. Validation of our metabolomics data in several human datasets and in cell line models provides a mechanistic basis for clinically assessing the ability of PaPEs to decrease breast cancer risk in obese postmenopausal women. Rewiring of key metabolic pathways by ERα has not been implicated in obesity-associated breast cancer before. Given the need for better strategies for preventing ER$^+$ breast cancers in obese postmenopausal women, our work offers both novel insights and a more complete understanding of the basic mechanisms that underlie the association of obesity and breast cancer. Our previous preclinical work, showing benefit of PaPE-1 to reduce risk of weight gain and metabolic syndrome associated with loss of estrogens (14), combined with our current work, highlight an actionable pharmacologic approach targeting ERα and mTOR signaling that can be exploited for future clinical translation. Our findings further emphasize the importance of weight loss strategies to reduce comorbidities associated with obesity, including breast cancer.

Disclosure of Potential Conflicts of Interest

Z. Madak-Erdogan reports receiving a commercial research grant from Pfizer and other commercial research support from Corteva Agrisciences. Z. Madak-Erdogan, J.A. Katzenellenbogen, and S.H. Kim are coinventors on several patents entitled "Novel Compounds Which Activate Estrogen Receptors and Compositions and Methods of Using the Same," which include protection of PaPE-1. Z. Madak-Erdogan was a principal investigator on an investigator-initiated grant from Corteva Agrisciences. No potential conflicts of interest were disclosed by the other authors.

Authors' Contributions

Conception and design: Z. Madak-Erdogan
Development of methodology: Z. Madak-Erdogan, S.H. Kim
Acquisition of data (provided animals, acquired and managed patients, provided facilities, etc.): Z. Madak-Erdogan, S. Band, Y.C. Zhao, E. Kulkoyluoglu-Cotul, Q. Zuo, A.S. Casiano, K. Wrobel, N. Marino, A.M.V. Storniolo, J.A. Flaws
Analysis and interpretation of data (e.g., statistical analysis, biostatistics, computational analysis): Z. Madak-Erdogan, Y.C. Zhao, G. Rossi, B.P. Smith, E. Kulkoyluoglu-Cotul, Q. Zuo, R.L. Smith, S.H. Kim, N. Marino, J.A. Flaws
Writing, review, and/or revision of the manuscript: Z. Madak-Erdogan, R.L. Smith, J.A. Katzenellenbogen, N. Marino, A.M.V. Storniolo, J.A. Flaws
Administrative, technical, or material support (i.e., reporting or organizing data, constructing databases): Z. Madak-Erdogan, S. Band, K. Wrobel, J.A. Katzenellenbogen, M.L. Johnson, M. Patel, N. Marino
Study supervision: Z. Madak-Erdogan

Acknowledgments

This work was supported by grants from the University of Illinois, Office of the Vice Chancellor for Research, College of ACES FIRE grant (to Z. Madak-Erdogan) and the National Institute of Food and Agriculture, U.S. Department of Agriculture, award ILLU-698-909 (to Z. Madak-Erdogan). We would like to thank to Dr. Alvaro Hernandez, Dr. Mark Band, and Dr. Chris Wright for assistance with RNASeq experiments. We would like to thank Dr. Gokhan Hotamisligil for his critical reading of our manuscript.

The costs of publication of this article were defrayed in part by the payment of page charges. This article must therefore be hereby marked *advertisement* in accordance with 18 U.S.C. Section 1734 solely to indicate this fact.

Received September 13, 2018; revised January 9, 2019; accepted March 8, 2019; published first March 12, 2019.

References

1. Islami F, Goding Sauer A, Gapstur SM, Jemal A. Proportion of cancer cases attributable to excess body weight by US state, 2011–2015. JAMA Oncol 2018 Dec 27 [Epub ahead of print].
2. Fryar CD, Kruszon-Moran D, Gu Q, Ogden CL. Mean body weight, height, waist circumference, and body mass index among adults: United States, 1999–2000 through 2015–2016. Natl Health Stat Reports 2018; 1–16.
3. Mauvais-Jarvis F, Clegg DJ, Hevener AL. The role of estrogens in control of energy balance and glucose homeostasis. Endocr Rev 2013;34:309–38.
4. Eliassen AH, Colditz GA, Rosner B, Willett WC, Hankinson SE. Adult weight change and risk of postmenopausal breast cancer. JAMA 2006; 296:193–201.
5. Suzuki R, Orsini N, Saji S, Key TJ, Wolk A. Body weight and incidence of breast cancer defined by estrogen and progesterone receptor status–a meta-analysis. Int J Cancer 2009;124:698–712.
6. van den Brandt PA, Spiegelman D, Yaun SS, Adami HO, Beeson L, Folsom AR, et al. Pooled analysis of prospective cohort studies on height, weight, and breast cancer risk. Am J Epidemiol 2000;152:514–27.
7. Yang XR, Chang-Claude J, Goode EL, Couch FJ, Nevanlinna H, Milne RL, et al. Associations of breast cancer risk factors with tumor subtypes: a pooled analysis from the Breast Cancer Association Consortium studies. J Natl Cancer Inst 2011;103:250–63.
8. Chan DS, Vieira AR, Aune D, Bandera EV, Greenwood DC, McTiernan A, et al. Body mass index and survival in women with breast cancer—systematic literature review and meta-analysis of 82 follow-up studies. Ann Oncol 2014;25:1901–14.
9. Fuentes-Mattei E, Velazquez-Torres G, Phan L, Zhang F, Chou PC, Shin JH, et al. Effects of obesity on transcriptomic changes and cancer hallmarks in estrogen receptor–positive breast cancer. J Natl Cancer Inst 2014;106:pii: dju158.
10. Park J, Morley TS, Kim M, Clegg DJ, Scherer PE. Obesity and cancer—mechanisms underlying tumour progression and recurrence. Nat Rev Endocrinol 2014;10:455–65.
11. Llaverias G, Danilo C, Mercier I, Daumer K, Capozza F, Williams TM, et al. Role of cholesterol in the development and progression of breast cancer. Am J Pathol 2011;178:402–12.
12. Nelson ER, Wardell SE, Jasper JS, Park S, Suchindran S, Howe MK, et al. 27-Hydroxycholesterol links hypercholesterolemia and breast cancer pathophysiology. Science 2013;342:1094–8.
13. Wu Q, Ishikawa T, Sirianni R, Tang H, McDonald Jeffrey G, Yuhanna IS, et al. 27-Hydroxycholesterol promotes cell-autonomous, ER-positive breast cancer growth. Cell Rep 2013;5:637–45.
14. Madak-Erdogan Z, Kim SH, Gong P, Zhao YC, Zhang H, Chambliss KL, et al. Design of pathway preferential estrogens that provide beneficial metabolic and vascular effects without stimulating reproductive tissues. Sci Signal 2016;9:ra53.
15. Ziv-Gal A, Smith RL, Gallicchio L, Miller SR, Zacur HA, Flaws JA. The Midlife Women's Health Study – a study protocol of a longitudinal prospective study on predictors of menopausal hot flashes. Womens Midlife Health 2017;3:4.
16. Nakshatri H, Anjanappa M, Bhat-Nakshatri P. Ethnicity-dependent and -independent heterogeneity in healthy normal breast hierarchy impacts tumor characterization. Sci Rep 2015;5:13526.
17. Polanska UM, Acar A, Orimo A. Experimental generation of carcinoma-associated fibroblasts (CAFs) from human mammary fibroblasts. J Vis Exp 2011:e3201. doi: 10.3791/3201.
18. Liu X, Ory V, Chapman S, Yuan H, Albanese C, Kallakury B, et al. ROCK inhibitor and feeder cells induce the conditional reprogramming of epithelial cells. Am J Pathol 2012;180:599–607.
19. Wrobel K, Zhao YC, Kulkoyluoglu E, Chen KL, Hieronymi K, Holloway J, et al. ERalpha-XPO1 cross talk controls tamoxifen sensitivity in tumors by altering ERK5 cellular localization. Mol Endocrinol 2016;30:1029–45.
20. Madak-Erdogan Z, Ventrella R, Petry L, Katzenellenbogen BS. Novel roles for ERK5 and cofilin as critical mediators linking ERalpha-driven transcription, actin reorganization, and invasiveness in breast cancer. Mol Cancer Res 2014;12:714–27.

21. Chong J, Soufan O, Li C, Caraus I, Li S, Bourque G, et al. MetaboAnalyst 4.0: towards more transparent and integrative metabolomics analysis. Nucleic Acids Res 2018;46:W486–94.
22. Granit RZ, Masury H, Condiotti R, Fixler Y, Gabai Y, Glikman T, et al. Regulation of cellular heterogeneity and rates of symmetric and asymmetric divisions in triple-negative breast cancer. Cell Rep 2018;24:3237–50.
23. Farren TW, Giustiniani J, Liu FT, Tsitsikas DA, Macey MG, Cavenagh JD, et al. Differential and tumor-specific expression of CD160 in B-cell malignancies. Blood 2011;118:2174–83.
24. Buchan SL, Rogel A, Al-Shamkhani A. The immunobiology of CD27 and OX40 and their potential as targets for cancer immunotherapy. Blood 2018;131:39–48.
25. Nunez AR. The role of the interleukin-12/STAT4 axis in breast cancer. J Immunol 2016;196(suppl 1):51.26.
26. Deng C, Lin YX, Qi XK, He GP, Zhang Y, Zhang HJ, et al. TNFRSF19 inhibits TGFβ signaling through interaction with TGFβ receptor type I to promote tumorigenesis. Cancer Res 2018;78:3469–83.
27. Kishi T, Grass L, Soosaipillai A, Scorilas A, Harbeck N, Schmalfeldt B, et al. Human kallikrein 8, a novel biomarker for ovarian carcinoma. Cancer Res 2003;63:2771–4.
28. DeRycke MS, Pambuccian SE, Gilks CB, Kalloger SE, Ghidouche A, Lopez M, et al. Nectin 4 overexpression in ovarian cancer tissues and serum: potential role as a serum biomarker. Am J Clin Pathol 2010;134:835–45.
29. White NM, Mathews M, Yousef GM, Prizada A, Popadiuk C, Doré JJ. KLK6 and KLK13 predict tumor recurrence in epithelial ovarian carcinoma. Br J Cancer 2009;101:1107–13.
30. Wong CH, Wu Z, Yu Q. CTSL2 is a pro-apoptotic target of E2F1 and a modulator of histone deacetylase inhibitor and DNA damage-induced apoptosis. Oncogene 2013;33:1249–57.
31. Akl MR, Nagpal P, Ayoub NM, Prabhu SA, Gliksman M, Tai B, et al. Molecular and clinical profiles of syndecan-1 in solid and hematological cancer for prognosis and precision medicine. Oncotarget 2015;6:28693–715.
32. Hsieh SL, Lin WW. Decoy receptor 3: an endogenous immunomodulator in cancer growth and inflammatory reactions. J Biomed Sci 2017;24:39.
33. Lauby-Secretan B, Scoccianti C, Loomis D, Grosse Y, Bianchini F, Straif K. Body fatness and cancer—viewpoint of the IARC Working Group. N Engl J Med 2016;375:794–8.
34. Jobard E, Pontoizeau C, Blaise BJ, Bachelot T, Elena-Herrmann B, Tredan O. A serum nuclear magnetic resonance-based metabolomic signature of advanced metastatic human breast cancer. Cancer Lett 2014;343:33–41.
35. Lai HS, Lee JC, Lee PH, Wang ST, Chen WJ. Plasma free amino acid profile in cancer patients. Semin Cancer Biol 2005;15:267–76.
36. Wei S, Liu L, Zhang J, Bowers J, Gowda GA, Seeger H, et al. Metabolomics approach for predicting response to neoadjuvant chemotherapy for breast cancer. Mol Oncol 2013;7:297–307.
37. Fay MP, Freedman LS, Clifford CK, Midthune DN. Effect of different types and amounts of fat on the development of mammary tumors in rodents: a review. Cancer Res 1997;57:3979–88.
38. Kleinfeld AM, Okada C. Free fatty acid release from human breast cancer tissue inhibits cytotoxic T-lymphocyte-mediated killing. J Lipid Res 2005;46:1983–90.
39. Quevedo-Coli S, Crespi C, Benito E, Palou A, Roca P. Alterations in circulating fatty acids and the compartmentation of selected metabolites in women with breast cancer. Biochem Mol Biol Int 1997;41:1–10.
40. Ewertz M, Jensen MB, Gunnarsdottir KA, Hojris I, Jakobsen EH, Nielsen D, et al. Effect of obesity on prognosis after early-stage breast cancer. J Clin Oncol 2011;29:25–31.
41. Chen X, Lu W, Zheng W, Gu K, Chen Z, Zheng Y, et al. Obesity and weight change in relation to breast cancer survival. Breast Cancer Res Treat 2010;122:823–33.
42. Loi S, Milne RL, Friedlander ML, McCredie MR, Giles GG, Hopper JL, et al. Obesity and outcomes in premenopausal and postmenopausal breast cancer. Cancer Epidemiol Biomarkers Prev 2005;14:1686–91.
43. Kerlikowske K, Walker R, Miglioretti DL, Desai A, Ballard-Barbash R, Buist DS. Obesity, mammography use and accuracy, and advanced breast cancer risk. J Natl Cancer Inst 2008;100:1724–33.
44. Hao J, Zhang Y, Yan X, Yan F, Sun Y, Zeng J, et al. Circulating adipose fatty acid binding protein is a new link underlying obesity-associated breast/mammary tumor development. Cell Metab 2018;28:689–705.
45. Wicha MS, Liotta LA, Kidwell WR. Effects of free fatty acids on the growth of normal and neoplastic rat mammary epithelial cells. Cancer Res 1979;39:426–35.
46. Goldberg IJ, Eckel RH, Abumrad NA. Regulation of fatty acid uptake into tissues: lipoprotein lipase- and CD36-mediated pathways. J Lipid Res 2009;50Suppl:S86–S90.
47. Hames KC, Vella A, Kemp BJ, Jensen MD. Free fatty acid uptake in humans with CD36 deficiency. Diabetes 2014;63:3606–14.
48. Huber AH, Kleinfeld AM. Unbound free fatty acid profiles in human plasma and the unexpected absence of unbound palmitoleate. J Lipid Res 2017;58:578–85.
49. Pascual G, Avgustinova A, Mejetta S, Martín M, Castellanos A, Attolini CS-O, et al. Targeting metastasis-initiating cells through the fatty acid receptor CD36. Nature 2017;541:41–5.
50. Tao Y, Pinzi V, Bourhis J, Deutsch E. Mechanisms of disease: signaling of the insulin-like growth factor 1 receptor pathway—therapeutic perspectives in cancer. Nat Clin Prac Oncol 2007;4:591–602.
51. Angela M, Endo Y, Asou HK, Yamamoto T, Tumes DJ, Tokuyama H, et al. Fatty acid metabolic reprogramming via mTOR-mediated inductions of PPARγ directs early activation of T cells. Nat Commun 2016;7:13683.
52. Michelet X, Dyck L, Hogan A, Loftus RM, Duquette D, Wei K, et al. Metabolic reprogramming of natural killer cells in obesity limits antitumor responses. Nat Immunol 2018;19:1330–40.
53. Yasuda M, Tanaka Y, Kume S, Morita Y, Chin-Kanasaki M, Araki H, et al. Fatty acids are novel nutrient factors to regulate mTORC1 lysosomal localization and apoptosis in podocytes. Biochim Biophys Acta 2014;1842:1097–108.
54. Menon D, Salloum D, Bernfeld E, Gorodetsky E, Akselrod A, Frias MA, et al. Lipid sensing by mTOR complexes via *de novo* synthesis of phosphatidic acid. J Biol Chem 2017;292:6303–11.
55. Arous C, Naïmi M, Van Obberghen E. Oleate-mediated activation of phospholipase D and mammalian target of rapamycin (mTOR) regulates proliferation and rapamycin sensitivity of hepatocarcinoma cells. Diabetologia 2011;54:954–64.